Chemically-induced swelling of hydrogels

John Dolbow,[†] Eliot Fried,[‡] Huidi Ji[†]

[†]Department of Civil and Environmental Engineering
Duke University
Durham, NC 27708-0287, USA

[‡]Department of Mechanical Engineering
Washington University in St. Louis
St. Louis, MO 63130-4899, USA

Abstract

We present a theory for the chemically-induced volume transitions of hydrogels. Consistent with experimental observations, we account for a sharp interface separating swelled and collapsed phases of the underlying polymer network. The polymer chains are treated as a solute with an associated diffusion potential and their concentration is assumed to be discontinuous across the interface. In addition to the standard bulk and interfacial equations imposing force balance and solute balance, the theory involves an ancillary interfacial equation imposing configurational force balance. Motivated by experimental observations, we specialize the theory to the situation where the time scale associated with the interface motion is slow compared to those associated with diffusion in the bulk phases. We present a hybrid eXtended-Finite-Element/Level-Set Method (XFE/LSM) for obtaining approximate solutions to the equations arising under this specialization. As an application, we consider the swelling of a spherical specimen whose boundary is traction-free and is in contact with a reservoir of uniform chemical potential. Our numerical results exhibit good qualitative comparison with experimental observations and predict characteristic swelling times that are proportional to the square of the specimen radius. Our results also suggest several possible synthetic pathways that might be pursued as a means to engineer hydrogels with optimal response times.

Keywords: A. Hydrogels; A. Phase transitions; A. Chemo-mechanical process; B. Configurational forces; B. Sharp interface

1 Introduction

Hydrogels are crosslinked, hydrophilic polymer networks whose composition can be tuned to exhibit large volumetric swelling in response to a variety of environmental stimuli. Importantly, hydrogels may act as both sensors and switches. When combined with the lack of a need for an external power source, this multifunctionality suggests a broad spectrum of applications. For example, hydrogels have recently been designed to serve as drug carriers/pumps in the bloodstream for therapeutic biomedical applications (Eichenbaum et al., 1999) and as microfluidic actuators (Beebe et al., 2000). But a lack of understanding of the relationship between gel composition and response kinetics has hindered the design of these materials and, accordingly, delayed the transfer of new applications from the laboratory to the marketplace. In this paper, we present a new theory for the chemo-mechanical response of hydrogels and demonstrate its predictive capabilities with the aid of advanced numerical methods.

For particular hydrogel compositions and external environmental conditions, a phase interface develops and the motion of this interface corresponds with the swelling response of the gel. The transition from a distinct collapsed phase to a swollen phase with the evolution of the interface was first observed by Tanaka (1978) for polyacrylamide-based hydrogels. The phenomenon is often referred to as a "volume transition" (Dušek, 1993) and a similar type of behavior has been observed by Budtova and Navard (1998) for polyelectrolyte gels in saline solutions. More recently, Olsen et al. (2000) developed a particle-imaging technique to observe the evolution of such hydrogel "microstructures." The importance of understanding this phenomenon rests on the fact that the kinetic response of hydrogels is directly coupled to the motion of the phase interface. Moreover, understanding the chemo-mechanical interaction between distinct phases facilitates the design of new hydrogels with specific drug release characteristics (Budtova, 1998).

In addition to the distinct phase transition exhibited by hydrogels, recent attention has focused on the "ripple" patterns observed on the surface of gel specimens during sufficiently large volumetric swelling or shrinking (Tanaka et al., 1987). The surface instability is initiated at the microscale, and the size of the associated cusps on the surface can expand to the characteristic size of the specimen itself. Indeed, rather dramatic changes in surface pattern have recently been observed on N-isopropylacrylamide (NIPA) gels as a function of temperature drift rate or superheating (Bai and Suzuki, 2000). These phenomena seem to mandate the need for models that account for curvature effects during the swelling process and, in addition, for the possibility of cusp formation on the interface during its evolution.

A significant number of phenomenological and empirical models have been developed to describe the swelling of hydrogels; a review of many of these can be found in Onuki (1993). With regard to representing the transition dynamics for multi-phase gels separated by a sharp interface, however, only a limited amount of previous research can be identified. Tomari and Doi (1994) developed a one-dimensional model that correlates with the experimental result of swelling times proportional to the square of gel radius. This model was later extended to the spherically symmetric case by Tomari and Doi (1995), where the authors employed a Flory–Huggins type free-energy functional for ionic gels in a neutral solution. For pH-sensitive gels, Gehrke et al. (1992) adopted a classical shrinking core model to cylindrical configurations and correlated their results to experimental measurements of the motion of the sharp ionization front. Their model did not consider large volume changes and the diffusion coefficients obtained from the correlation process were found to be significantly lower than those reported elsewhere.

In the majority of the above cases, the "collective diffusion" assumption proposed by Tanaka et al. (1973) was invoked. Collective diffusion assumes that swelling occurs simultaneously throughout the medium. Under this assumption, the characteristic time of swelling is incorporated by modifying the force balance to consider the "frictional force" acting between the polymer network and the solute. This yields a parabolic governing equation that, indeed, predicts collective diffusion. Swelling times obtained using this approach do correlate reasonably well with experimental results. However, in contrast with the assumptions underlying this approach, the observations of Olsen et al. (2000) show clearly that swelling proceeds with the propagation of interfaces separating swelled and collapsed phases.

In this paper, we present a theory which accounts for the role of interface propagation in the chemo-mechanical swelling of hydrogels. Faced with the task of developing such a theory, we adopt the perspective of Gibbs (1878), who modeled phase interfaces as surfaces across which the material properties of the bulk phases may suffer discontinuities and, to account for localized interactions between phases, endowed these surfaces with excess fields. The structure of our theory closely resembles a theory developed by Gurtin and Voorhees (1993) for diffusional phase transitions in crystalline solids. Of key importance in this theory is an interfacial equation, expressing configurational force balance (Gurtin and Struthers, 1990; Gurtin, 1995; Gurtin, 2000), which generalizes the

Gibbs–Thomson relation arising in descriptions of alloy solidification (cf., e.g., Mullins and Sekerka (1963)) and supplements the conventional equations which express mass balance and standard force balance in the bulk phases and across the interface.

A number of alternative strategies have been advocated for the construction of approximate numerical solutions to problems arising in sharp-interface models for phase transitions. As it is not our intention to provide a comprehensive account of these methods, we refer the reader to the recent review of Udaykumar et al. (1999). The main point is that optimal rates of convergence in suitable error norms can be obtained for these problems only if the numerical approximation retains the sharp interface representation. Within the context of finite-element approximations, this result imposes overly restrictive conditions on the mesh. Until recently, one of the few strategies for capturing the local discontinuities near an evolving sharp interface was to adopt moving-mesh formulations akin to those developed in the pioneering work of Lynch and O'Neill (1981). Among the many concerns with such formulations is the potential for severe mesh distortion, especially in two- and three-dimensional problems where the geometry of the interface is generally non-planar.

The eXtended-Finite-Element Method (X-FEM) (Moës et al., 1999; Dolbow, 1999) is a variation on the partition-of-unity framework (Melenk and Babuška, 1996) for building local, non-polynomial ansatz spaces into an approximation. A further variation on this theme concerns the eXtended-Finite-Element/Level-Set Method (XFE/LSM), wherein both the local solution and geometry of arbitrarily evolving features are represented with evolving functions. The coupling of the two methods was first conceived in Sukumar et al. (2001), albeit for stationary geometric features. Recently, the XFE/LSM has been employed to simulate phase transition problems where the interface is assumed to be sharp. Merle and Dolbow (2002) developed a one-dimensional formulation for Stefan problems and Ji et al. (2002) recently generalized this approach to multi-dimensional solidification problems. In this paper, the basic techniques are extended to account for the finite strains associated with the extreme ($\sim 1000\%$) volumetric change possible in hydrogels. Central to our approach is the use of discontinuous enrichment functions to capture discontinuities in the gradients of the deformation and the diffusion potential across the phase interface. Lagrange multipliers are employed to satisfy additional constraints at the interface and the multipliers are subsequently used to interpret the pertinent flux quantities. This allows for the accurate simulation of the evolution of the phase interface without recourse to remeshing or moving mesh techniques. It is also qualitatively different from previous numerical strategies (Tomari and Doi, 1994; Tomari and Doi, 1995), strategies wherein the interface is smeared over a single element.

As an elementary application of the theory presented here, we consider the case of a spherical specimen subjected to purely radial chemo-mechanical boundary conditions. In particular, the boundary of the specimen is assumed to be traction free and in contact with a solvent-rich reservoir within which the diffusion potential is spatially uniform but may vary in time. We seek solutions in which the deformation and diffusion potential are assumed to be radially symmetric. This leads to a nonlinear initial-boundary-value problem which we solve numerically using the XFE/LSM method.

This paper is organized as follows. In Section 2, we develop a theoretical framework capable of describing a gel subjected to combined mechanical and chemical loading. This framework is based upon balances for deformational force, configurational force, and solute concentration as well as a dissipation imbalance that, in the isothermal context to which we confine our attention, imposes the first and second laws of thermodynamics. Section 3 then presents a specialization of the theory that invokes a number of simplifying assumptions. Section 4 describes the variational form of a generic mixed boundary-value problem and the discretization with the XFE/LSM. In Section 5, we consider a spherically symmetric specimen subjected to purely radial loadings and provide the numerical results obtained by our algorithm. Finally, a summary of our results and discussion of future directions are provided in Section 6.

2 Background

Our approach to the basic theory follows closely that of Gurtin and Voorhees (1993), except that, to account for the extreme distortions that occur during the swelling of hydrogels, we allow for finite strains.

2.1 Kinematics

We consider a two-phase body identified with a bounded region $\mathcal{R}$ of three-dimensional Euclidean point space that it occupies in a fixed reference configuration. Labeling the swelled and collapsed phases by α and β, respectively, we assume that for each t: $\mathcal{R}$ is separated by a interface $\mathcal{S}(t)$ into complementary subregions $\mathcal{R}_\alpha(t)$ and $\mathcal{R}_\beta(t)$ occupied by phases α and β.

The theory requires two types of fields:

- bulk fields, defined on $\mathcal{R}_\alpha(t)$ and $\mathcal{R}_\beta(t)$ for all t, which characterize behavior within the two phases;
- interfacial fields, defined on $\mathcal{S}(t)$ for all t, which characterize the behavior of the interface.

Given a bulk field g, we use $\overset{-}{g}$ and $\overset{+}{g}$ to denote the limits of g as the interface is approached from the α- and β-phase regions, $[\![g]\!]$ to denote the jump of g across the interface, and $\langle\!\langle g\rangle\!\rangle$ to denote the average of g across the interface. Thus, for $\mathbf{x}$ on $\mathcal{S}(t)$,

$$\left.\begin{aligned}\overset{-}{g}(\mathbf{x},t) &= \lim_{\substack{\boldsymbol{\xi}\to\mathbf{x}\\ \boldsymbol{\xi}\in\mathcal{R}_\alpha(t)}} g(\boldsymbol{\xi},t), &\qquad \overset{+}{g}(\mathbf{x},t) &= \lim_{\substack{\boldsymbol{\xi}\to\mathbf{x}\\ \boldsymbol{\xi}\in\mathcal{R}_\beta(t)}} g(\boldsymbol{\xi},t),\\ [\![g]\!](\mathbf{x},t) &= \overset{+}{g}(\mathbf{x},t)-\overset{-}{g}(\mathbf{x},t), &\qquad \langle\!\langle g\rangle\!\rangle(\mathbf{x},t) &= \tfrac{1}{2}\big(\overset{+}{g}(\mathbf{x},t)+\overset{-}{g}(\mathbf{x},t)\big).\end{aligned}\right\} \tag{2.1}$$

We confine our attention to circumstances under which $\mathcal{S}(t)$ is, for each t, a smoothly orientable surface that evolves smoothly in time. We write $\mathbf{n}$ for the unit normal on $\mathcal{S}$, directed outward from $\mathcal{R}_\alpha$ as shown in Figure 1,

$$\mathbf{P} = \mathbf{I} - \mathbf{n}\otimes\mathbf{n} \tag{2.2}$$

for the projector on $\mathcal{S}$, and

$$\mathbf{v} = \mathsf{v}\mathbf{n} \tag{2.3}$$

for the scalar and vector normal velocities of $\mathcal{S}$.

We use Grad and $\mathrm{Grad}_{\mathcal{S}}$ to denote the gradient operators in bulk and on the interface, with the associated divergence operators being Div and $\mathrm{Div}_{\mathcal{S}}$. In particular,

$$\mathbf{L} = -\mathrm{Grad}_{\mathcal{S}}\mathbf{n} \qquad \text{and} \qquad \mathsf{K} = \mathbf{P}\cdot\mathbf{L} = \mathrm{tr}\,\mathbf{L} = -\mathrm{Div}_{\mathcal{S}}\mathbf{n} \tag{2.4}$$

denote the curvature tensor and total curvature (i.e., twice the mean curvature) of $\mathcal{S}$. Further, we use a superposed dot to denote differentiation with respect to time with position in bulk held fixed and a superposed box to denote differentiation with respect to

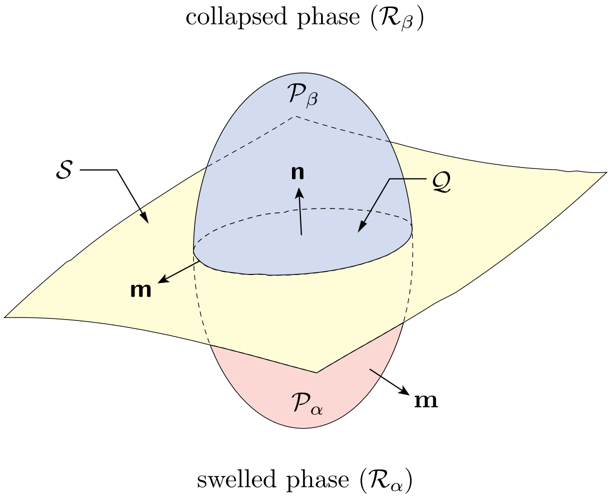

Figure 1: Schematic indicating: the regions occupied by the swelled and collapsed phases; the evolving interface $\mathcal{S}$, with unit normal $\boldsymbol{\mathsf{n}}$ directed into the collapsed phase; a fixed control volume $\mathcal{P}$, with outward unit normal $\mathbf{m}$, divided by $\mathcal{S}$ into time-dependent regions $\mathcal{P}_\alpha$ and $\mathcal{P}_\beta$ in the swelled and collapsed phases; and the portion $\mathcal{Q} = \mathcal{P} \cap \mathcal{S}$ of $\mathcal{S}$, with outward unit binormal $\boldsymbol{\mathsf{m}}$, contained within $\mathcal{P}$.

time following the normal trajectories of the interface. The orientation $\boldsymbol{\mathsf{n}}$ and the scalar normal-velocity v are then related by the identity

$$\overset{\scriptscriptstyle\square}{\boldsymbol{\mathsf{n}}} = -\mathrm{Grad}_{\mathcal{S}}\mathsf{v}. \tag{2.5}$$

We write $\mathbf{y}$ for the motion of the body. Basic to the theory is the assumption of coherence,

$$[\![\mathbf{y}]\!] = \mathbf{0}, \tag{2.6}$$

which requires that the motion be continuous across the phase interface. Introducing the deformation gradient $\mathbf{F} = \mathrm{Grad}\,\mathbf{y}$ and the velocity $\dot{\mathbf{y}}$, we have, as consequences of this assumption, the compatibility conditions

$$[\![\mathbf{F}]\!]\boldsymbol{\mathsf{P}} = \mathbf{0} \qquad \text{and} \qquad [\![\dot{\mathbf{y}}]\!] + [\![\mathbf{F}]\!]\boldsymbol{\mathsf{v}} = \mathbf{0}. \tag{2.7}$$

Motivated by the coherency condition (2.6), we introduce the interfacial deformation $\boldsymbol{\mathsf{y}} = \mathbf{y}|_{\mathcal{S}}$ and the interfacial deformation gradient

$$\boldsymbol{\mathsf{F}} = \mathrm{Grad}_{\mathcal{S}}\boldsymbol{\mathsf{y}}. \tag{2.8}$$

Direct calculations based on the compatibility conditions (2.7) then show that

$$\mathrm{Grad}_{\mathcal{S}}\boldsymbol{\mathsf{y}} = \boldsymbol{\mathsf{A}}\boldsymbol{\mathsf{P}} \qquad \text{and} \qquad \overset{\scriptscriptstyle\square}{\boldsymbol{\mathsf{y}}} = \langle\!\langle \dot{\mathbf{y}} \rangle\!\rangle + \boldsymbol{\mathsf{A}}\boldsymbol{\mathsf{v}}, \tag{2.9}$$

with

$$\boldsymbol{\mathsf{A}} = \langle\!\langle \mathbf{F} \rangle\!\rangle \tag{2.10}$$

the interfacial average of the deformation gradient.

2.2 Mechanics

In addition to deformational forces associated with the motion of material particles, we account for configurational forces (Gurtin and Struthers, 1990; Gurtin, 1995; Gurtin, 2000) associated with the motion of the nonmaterial interface separating the swelled and collapsed phases. We neglect inertia and external body forces.

To state the fundamental balances, we work with an arbitrary fixed control-volume $\mathcal{P}$ with outward unit normal $\mathbf{m}$, as depicted in Figure 1. Further, using $\mathcal{Q}(t) = \mathcal{P} \cap \mathcal{S}(t)$ to denote the (possibly empty) portion of the interface that lies within $\mathcal{P}$ at time t, we write $\boldsymbol{\mathsf{m}}$ for the unit binormal to $\partial\mathcal{Q}$ and w for the tangential edge-velocity of $\partial\mathcal{Q}$ in the direction of $\boldsymbol{\mathsf{m}}$.

2.2.1 Deformational force balance

Since we neglect external force, the deformational force system consists only of the bulk and interfacial deformational stresses $\mathbf{S}$ and $\boldsymbol{\mathsf{S}}$.[1] The deformational force and moment balances are therefore expressed by the requirement that

$$\int\limits_{\partial\mathcal{P}} \mathbf{S}\mathbf{m}\,da + \int\limits_{\partial\mathcal{Q}} \boldsymbol{\mathsf{S}}\boldsymbol{\mathsf{m}}\,dl = \mathbf{0} \tag{2.11}$$

and

$$\int\limits_{\partial\mathcal{P}} \mathbf{y}\times\mathbf{S}\mathbf{m}\,da + \int\limits_{\partial\mathcal{Q}} \mathbf{y}\times\boldsymbol{\mathsf{S}}\boldsymbol{\mathsf{m}}\,dl = \mathbf{0} \tag{2.12}$$

hold for all $\mathcal{P}$ and all time. Using the bulk and interfacial divergence theorems along with the arbitrary nature of $\mathcal{P}$, we localize these balances to obtain the classical bulk relations

$$\mathrm{Div}\,\mathbf{S} = \mathbf{0} \qquad \text{and} \qquad \mathbf{S}\mathbf{F}^{\top} = \mathbf{F}\mathbf{S}^{\top} \tag{2.13}$$

and the interfacial relations

$$[\![\mathbf{S}]\!]\boldsymbol{\mathsf{n}} + \mathrm{Div}_{\mathcal{S}}\boldsymbol{\mathsf{S}} = \mathbf{0} \qquad \text{and} \qquad \boldsymbol{\mathsf{S}}\boldsymbol{\mathsf{F}}^{\top} = \boldsymbol{\mathsf{F}}\boldsymbol{\mathsf{S}}^{\top}. \tag{2.14}$$

2.2.2 Configurational force balance

The configurational force system consists of a bulk configurational stress $\mathbf{C}$, a bulk configurational force density $\mathbf{f}$, an interfacial configurational stress $\boldsymbol{\mathsf{C}}$, and an interfacial configurational force density $\boldsymbol{\mathsf{f}}$.[2] We assume that these fields comply with the configurational force balance

$$\int\limits_{\partial\mathcal{P}} \mathbf{C}\mathbf{m}\,da + \int\limits_{\mathcal{P}} \mathbf{f}\,dv + \int\limits_{\partial\mathcal{Q}} \boldsymbol{\mathsf{C}}\boldsymbol{\mathsf{m}}\,dl + \int\limits_{\mathcal{Q}} \boldsymbol{\mathsf{f}}\,da = \mathbf{0} \tag{2.15}$$

for all $\mathcal{P}$ and all time. Using the bulk and interfacial divergence theorems, this balance localizes to yield the bulk relation

$$\mathrm{Div}\,\mathbf{C} + \mathbf{f} = \mathbf{0} \tag{2.16}$$

---

[1] The interfacial stress $\boldsymbol{\mathsf{S}}$ is superfical (Gurtin and Struthers, 1990; Gurtin, 2000) in the sense that $\boldsymbol{\mathsf{S}}\boldsymbol{\mathsf{n}} = \mathbf{0}$.

[2] Like $\boldsymbol{\mathsf{S}}$, $\boldsymbol{\mathsf{C}}$ obeys $\boldsymbol{\mathsf{C}}\boldsymbol{\mathsf{n}} = \mathbf{0}$.

and the interfacial relation

$$[\![\mathbf{C}]\!]\mathbf{n} + \mathrm{Div}_{\mathcal{S}}\mathbf{C} + \mathbf{f} = \mathbf{0}. \tag{2.17}$$

Introducing the decompositions

$$\mathbf{C} = \mathbf{C}_{\tan} + \mathbf{n}\otimes\mathbf{c}, \qquad \begin{cases} \mathbf{C}_{\tan} = \mathbf{P}\mathbf{C}, \\ \quad\;\; \mathbf{c} = \mathbf{C}^{\top}\mathbf{n}, \end{cases} \tag{2.18}$$

and

$$\mathbf{f} = \mathbf{f}_{\tan} + \mathsf{f}\mathbf{n}, \qquad \begin{cases} \mathbf{f}_{\tan} = \mathbf{P}\mathbf{f}, \\ \quad\; \mathsf{f} = \mathbf{f}\cdot\mathbf{n}. \end{cases} \tag{2.19}$$

we obtain from (2.17) the normal configurational force balance

$$\mathbf{n}\cdot[\![\mathbf{C}]\!]\mathbf{n} + \mathbf{C}_{\tan}\cdot\mathbf{L} + \mathrm{Div}_{\mathcal{S}}\mathbf{c} + \mathsf{f} = 0, \tag{2.20}$$

which is of central importance in the theory.

2.3 Solute balance

We treat the polymer chains as a solute with concentration c and flux $\mathbf{h}$. Neglecting diffusion within the interface, solute balance is the requirement that

$$\dot{\overline{\int_{\mathcal{P}} c\,dv}} = -\int_{\partial\mathcal{P}} \mathbf{h}\cdot\mathbf{m}\,da \tag{2.21}$$

for all $\mathcal{P}$ and all time. Using the bulk transport and divergence theorems, this balance localizes to yield the classical bulk relation

$$\dot{c} = -\mathrm{Div}\,\mathbf{h} \tag{2.22}$$

and the interfacial relation

$$\mathsf{v}[\![c]\!] = [\![\mathbf{h}]\!]\cdot\mathbf{n}. \tag{2.23}$$

2.4 Energetics

2.4.1 Energy densities. Total energy of a control volume

Introducing the bulk free-energy density Ψ and the interfacial free-energy density $\mathsf{\Psi}$, the net free-energy of $\mathcal{P}$ is

$$\int_{\mathcal{P}} \Psi\,dv + \int_{\mathcal{Q}} \mathsf{\Psi}\,da. \tag{2.24}$$

Thus, accounting for energy transport across $\partial\mathcal{Q}$ as the interface propagates through $\mathcal{P}$, the rate at which the free-energy in $\mathcal{P}$ changes with respect to time is

$$\dot{\overline{\int_{\mathcal{P}} \Psi\,dv + \int_{\mathcal{Q}} \mathsf{\Psi}\,da}} - \int_{\partial\mathcal{Q}} \mathsf{\Psi}\mathsf{w}\,dl. \tag{2.25}$$

2.4.2 Diffusion potential. Energy inflow due to solute transport

To account for changes in energy associated with solute transport, we introduce a diffusion potential u. The energy carried into $\mathcal{P}$ by the transport of solute across $\partial\mathcal{P}$ is then

$$-\int\limits_{\partial\mathcal{P}} u\mathbf{h}\cdot\mathbf{m}\,da. \tag{2.26}$$

Basic to our theory is the assumption of local chemical equilibrium,

$$[\![u]\!] = 0, \tag{2.27}$$

which requires that the diffusion potential be continuous across the interface. Motivated by (2.27), we introduce the interfacial diffusion potential

$$\mathsf{u} = u|_{\mathcal{S}}. \tag{2.28}$$

2.4.3 Power

The power expended on $\mathcal{P}$ must account not only for the working of the deformational traction $\mathbf{Sm}$ distributed over the boundary $\partial\mathcal{P}$ of the control volume, but also for the workings of the deformational traction $\boldsymbol{\mathsf{Sm}}$ and the configurational traction $\boldsymbol{\mathsf{Cm}}$ distributed over the curve $\partial\mathcal{Q}$ formed by the intersection of the interface $\mathcal{S}$ with $\partial\mathcal{P}$. As a material surface, $\mathcal{P}$ may be described intrinsically in terms of the motion. The traction $\mathbf{Sm}$ is therefore power-conjugate to the associated material velocity $\dot{\mathbf{y}}$. By analogy, we expect that the interfacial deformational traction $\boldsymbol{\mathsf{Sm}}$ should be power-conjugate to the motion velocity $\overset{\square}{\boldsymbol{\mathsf{y}}}$ following the interface (Gurtin and Struthers, 1990; Gurtin, 1995; Gurtin, 2000). On the other hand, the configurational traction $\boldsymbol{\mathsf{Cm}}$ is associated with the change in material structure accompanying the evolution of the phase interface and is thus power-conjugate to the intrinsic velocity $\boldsymbol{\mathsf{v}} = \mathsf{v}\boldsymbol{\mathsf{n}}$ of the interface (Gurtin and Struthers, 1990; Gurtin, 1995; Gurtin, 2000). Thus, bearing in mind that $\mathcal{P}$ is fixed (whereby there is no working associated with the configurational traction $\mathbf{Cm}$ over $\partial\mathcal{P}$), it follows that the total power expended on $\mathcal{P}$ by external agencies is

$$\int\limits_{\partial\mathcal{P}} \mathbf{Sm}\cdot\dot{\mathbf{y}}\,da + \int\limits_{\partial\mathcal{Q}} \big(\boldsymbol{\mathsf{Sm}}\cdot\overset{\square}{\boldsymbol{\mathsf{y}}} + \boldsymbol{\mathsf{Cm}}\cdot\boldsymbol{\mathsf{v}}\big)\,dl, \tag{2.29}$$

which, in view of (2.3) and the decomposition (2.18), can be written alternatively as

$$\int\limits_{\partial\mathcal{P}} \mathbf{Sm}\cdot\dot{\mathbf{y}}\,da + \int\limits_{\partial\mathcal{Q}} \big(\boldsymbol{\mathsf{Sm}}\cdot\overset{\square}{\boldsymbol{\mathsf{y}}} + \boldsymbol{\mathsf{c}}\cdot(\mathsf{v}\boldsymbol{\mathsf{m}})\big)\,dl. \tag{2.30}$$

2.4.4 Free-energy imbalance

We confine our attention to isothermal circumstances. The first and second laws of thermodynamics then combine to yield a free-energy imbalance which requires that, for each control volume $\mathcal{P}$ and each time, the rate of change of the free energy of $\mathcal{P}$ not exceed the sum of the energy carried into $\mathcal{P}$ by bulk diffusion across its boundary and the power expended on $\mathcal{P}$ by external agencies. Bearing in mind (2.25), (2.26), and (2.30), free-energy imbalance is the requirement that

$$\overset{\displaystyle\cdot}{\overline{\int\limits_{\mathcal{P}} \Psi\,dv + \int\limits_{\mathcal{Q}} \Psi\,da}} - \int\limits_{\partial\mathcal{Q}} \Psi\mathsf{w}\,dl \le -\int\limits_{\partial\mathcal{P}} u\mathbf{h}\cdot\mathbf{m}\,da + \int\limits_{\partial\mathcal{P}} \mathbf{Sm}\cdot\dot{\mathbf{y}}\,da + \int\limits_{\partial\mathcal{Q}} (\boldsymbol{\mathsf{Sm}}\cdot\overset{\square}{\boldsymbol{\mathsf{y}}} + (\boldsymbol{\mathsf{c}}\cdot\boldsymbol{\mathsf{m}})\mathsf{v})\,dl \tag{2.31}$$

for all $\mathcal{P}$ and all time. In view of bulk transport theorem and its interfacial counterpart (Gurtin, 1995), the bulk and interfacial divergence theorems, the bulk balances $(2.13)_1$ and (2.22), the kinematic identities $(2.4)_2$, (2.5), $(2.7)_2$, and $(2.9)_2$, the commutator identity (Gurtin, 2000)

$$\mathrm{Grad}_{\mathcal{S}}\overset{\square}{\boldsymbol{\mathsf{y}}} = \overset{\square}{\boldsymbol{\mathsf{F}}} + \boldsymbol{\mathsf{F}}\overset{\square}{\boldsymbol{\mathsf{n}}}\otimes\boldsymbol{\mathsf{n}} - \mathsf{v}\boldsymbol{\mathsf{FL}} = \overset{\square}{\boldsymbol{\mathsf{A}}}\boldsymbol{\mathsf{P}} - \boldsymbol{\mathsf{An}}\otimes\overset{\square}{\boldsymbol{\mathsf{n}}} - \mathsf{v}\boldsymbol{\mathsf{FL}}, \tag{2.32}$$

and the interfacial balances $(2.14)_1$, (2.20), and (2.23), the imbalance (2.31) localizes to yield the familiar bulk free-energy inequality

$$\dot{\Psi} - u\dot{c} - \mathbf{S}\cdot\dot{\mathbf{F}} + \mathbf{h}\cdot\mathrm{Grad}\,u \le 0 \tag{2.33}$$

and, as well, the interfacial free-energy inequality

$$\overset{\square}{\mathsf{\Psi}} - \boldsymbol{\mathsf{S}}\cdot\overset{\square}{\boldsymbol{\mathsf{A}}} + \boldsymbol{\mathsf{p}}\cdot\overset{\square}{\boldsymbol{\mathsf{n}}} + (\mathsf{f} + \boldsymbol{\mathsf{n}}\cdot[\![\mathbf{D}]\!]\boldsymbol{\mathsf{n}} + \boldsymbol{\mathsf{D}}\cdot\boldsymbol{\mathsf{L}})\mathsf{v} \le 0, \tag{2.34}$$

where we have introduced

$$\boldsymbol{\mathsf{p}} = \boldsymbol{\mathsf{c}} + \boldsymbol{\mathsf{A}}^{\top}\boldsymbol{\mathsf{Sn}}, \quad \mathbf{D} = \mathbf{C} - (\Psi - cu)\mathbf{I} + \mathbf{F}^{\top}\mathbf{S}, \quad \text{and} \quad \boldsymbol{\mathsf{D}} = \boldsymbol{\mathsf{C}}_{\tan} - \mathsf{\Psi}\boldsymbol{\mathsf{P}} + \boldsymbol{\mathsf{F}}^{\top}\boldsymbol{\mathsf{S}}. \tag{2.35}$$

2.5 Eshelby relations

If, following Gurtin (1995, 2000), we consider the free-energy imbalance for a migratrating control-volume, the requirement that the imbalance be invariant under changes of parameterization of the boundary of that volume implies that the bulk configurational stress is given by the classical Eshelby relation

$$\mathbf{C} = (\Psi - cu)\mathbf{I} - \mathbf{F}^{\top}\mathbf{S} \tag{2.36}$$

and that the tangential component $\boldsymbol{\mathsf{C}}_{\tan}$ of the interfacial configurational stress $\boldsymbol{\mathsf{C}}$ is given by the analogous relation

$$\boldsymbol{\mathsf{C}}_{\tan} = \mathsf{\Psi}\boldsymbol{\mathsf{P}} - \boldsymbol{\mathsf{F}}^{\top}\boldsymbol{\mathsf{S}}. \tag{2.37}$$

In view of (2.36) and (2.37), $\mathbf{D}$ and $\boldsymbol{\mathsf{D}}$ as defined in $(2.35)_2$ vanish and the interfacial free-energy inequality (2.34) reduces to

$$\overset{\square}{\mathsf{\Psi}} - \boldsymbol{\mathsf{S}}\cdot\overset{\square}{\boldsymbol{\mathsf{A}}} + \boldsymbol{\mathsf{p}}\cdot\overset{\square}{\boldsymbol{\mathsf{n}}} + \mathsf{f}\mathsf{v} \le 0, \tag{2.38}$$

2.6 Constitutive equations

2.6.1 Bulk constitutive equations

Our framework for bulk constitutive equations follows those presented by Gurtin and Voorhees (1993) and Fried and Gurtin (1999), excepting that we account for finite strains. Introducing the Gibbs-energy density

$$\Omega = \Psi - cu, \tag{2.39}$$

we rewrite the bulk free-energy inequality (2.33) as

$$\dot{\Omega} + c\dot{u} - \mathbf{S}\cdot\dot{\mathbf{F}} + \mathbf{h}\cdot\mathrm{Grad}\,u \le 0 \tag{2.40}$$

and assume that, in each phase $\gamma = \alpha, \beta$,

$$\Omega = \Omega_{\gamma}(\mathbf{F}, u), \qquad \mathbf{S} = \frac{\partial\Omega_{\gamma}(\mathbf{F}, u)}{\partial\mathbf{F}}, \qquad c = -\frac{\partial\Omega_{\gamma}(\mathbf{F}, u)}{\partial u}, \tag{2.41}$$

with Ω_γ suitably smooth, and

$$\mathbf{h} = -\mathbf{M}_\gamma(\mathbf{F}, u)\operatorname{Grad} u, \tag{2.42}$$

with the molecular mobility tensor $\mathbf{M}_\gamma$ positive-definite, viz.,

$$\mathbf{g}\cdot\mathbf{M}_\gamma(\mathbf{F}, u)\mathbf{g} > 0 \qquad \text{for all } \mathbf{g}. \tag{2.43}$$

To account for the isotropy of a gel-like substance, we assume that

$$\Omega_\gamma(\mathbf{F}, u) = \hat{\Omega}_\gamma(\imath(\mathbf{B}), u) \tag{2.44}$$

and that

$$\mathbf{M}_\gamma(\mathbf{F}, u) = \hat{M}_0^\gamma(\imath(\mathbf{B}), u)\mathbf{I} + \hat{M}_1^\gamma(\imath(\mathbf{B}), u)\mathbf{B} + \hat{M}_2^\gamma(\imath(\mathbf{B}), u)\mathbf{B}^2, \tag{2.45}$$

where $\mathbf{B} = \mathbf{F}\mathbf{F}^\top$ is the left Cauchy–Green tensor and

$$\imath(\mathbf{B}) = (I_1(\mathbf{B}), I_2(\mathbf{B}), I_3(\mathbf{B})), \tag{2.46}$$

with

$$I_1(\mathbf{B}) = \operatorname{tr}\mathbf{B}, \quad I_2(\mathbf{B}) = \tfrac{1}{2}(I_1^2(\mathbf{B}) - I_1(\mathbf{B}^2)), \quad \text{and} \quad I_3(\mathbf{B}) = \det\mathbf{B} \tag{2.47}$$

the principal invariants $\mathbf{B}$.

2.6.2 Interfacial constitutive equations

Turning to the interface, we assume that Ψ, S, p, and f are determined constitutively by smooth functions of A and v.[3] It follows that the inequality (2.38) holds if and only if

$$\Psi = \tilde{\Psi}(\mathsf{A}), \qquad \mathsf{S} = \frac{\partial\tilde{\Psi}(\mathsf{A})}{\partial\mathsf{A}}, \qquad \mathsf{p} = \mathbf{0}, \tag{2.48}$$

and

$$\mathsf{f} = -\mathsf{b}(\mathsf{A}, \mathsf{v})\mathsf{v}, \tag{2.49}$$

where b must satisfy

$$\mathsf{b}(\mathsf{A}, \mathsf{v}) \geq 0. \tag{2.50}$$

Consistent with our treatment of the bulk phases, we assume that the interfacial constitutive response is isotropic, so that

$$\tilde{\Psi}(\mathsf{A}) = \hat{\Psi}(\imath(\mathsf{A}\mathsf{A}^\top)) \quad \text{and} \quad \mathsf{b}(\mathsf{A}, \mathsf{v}) = \hat{\mathsf{b}}(\imath(\mathsf{A}\mathsf{A}^\top), \mathsf{v}). \tag{2.51}$$

---

[3] For an anisotropic material, it would also be reasonable to allow for constitutive dependence on the interfacial orientation n. The constitutive framework considered here is therefore a specialization of that developed by Gurtin (2000, §21e) for anisotropic materials.

2.7 Evolution equations

Combining the bulk constitutive equations (2.41) and (2.42) with the bulk deformational force balance $(2.13)_1$ and mass balance (2.22) yields equations,

$$\left.\begin{aligned} \mathrm{Div}\Big(\frac{\partial\Omega_\gamma(\mathbf{F},u)}{\partial\mathbf{F}}\Big) &= \mathbf{0}, \\ \dot{\overline{\frac{\partial\Omega_\gamma(\mathbf{F},u)}{\partial u}}} &= -\mathrm{Div}\,(\mathbf{M}_\gamma(\mathbf{F},u)\mathrm{Grad}\,u), \end{aligned}\right\} \tag{2.52}$$

on the evolving regions $\mathcal{R}_\gamma$ occupied by the bulk phases $\gamma = \alpha, \beta$. Similarly, combining the bulk and interfacial constitutive equations (2.41), (2.42), (2.48), and (2.49) with the interfacial deformational force balance $(2.14)_1$ and mass balance (2.23) yields equations,

$$\left.\begin{aligned} \Big\llbracket\frac{\partial\Omega_\gamma(\mathbf{F},u)}{\partial\mathbf{F}}\Big\rrbracket\boldsymbol{\mathsf{n}} + \mathrm{Div}_{\mathcal{S}}\Big(\frac{\partial\tilde{\Psi}(\boldsymbol{\mathsf{A}})}{\partial\boldsymbol{\mathsf{A}}}\Big) &= \mathbf{0}, \\ \mathsf{v}\Big\llbracket\frac{\partial\Omega_\gamma(\mathbf{F},u)}{\partial u}\Big\rrbracket &= \llbracket\mathbf{M}_\gamma(\mathbf{F},u)\mathrm{Grad}\,u\rrbracket\cdot\boldsymbol{\mathsf{n}}, \end{aligned}\right\} \tag{2.53}$$

on the evolving phase interface $\mathcal{S}$. The normal configurational force balance (2.20) yields an additional evolution equation,

$$\begin{aligned} \boldsymbol{\mathsf{n}}\cdot\Big\llbracket\Omega_\gamma(\mathbf{F},u)\mathbf{I} - \mathbf{F}^\top\frac{\partial\Omega_\gamma(\mathbf{F},u)}{\partial\mathbf{F}}\Big\rrbracket\boldsymbol{\mathsf{n}} + \Big(\tilde{\Psi}(\boldsymbol{\mathsf{A}})\boldsymbol{\mathsf{P}} - \boldsymbol{\mathsf{F}}^\top\frac{\partial\tilde{\Psi}(\boldsymbol{\mathsf{A}})}{\partial\boldsymbol{\mathsf{A}}}\Big)\cdot\boldsymbol{\mathsf{L}} \\ + \mathrm{Div}_{\mathcal{S}}\Big(\Big(\frac{\partial\tilde{\Psi}(\boldsymbol{\mathsf{A}})}{\partial\boldsymbol{\mathsf{A}}}\Big)^\top\boldsymbol{\mathsf{A}}\boldsymbol{\mathsf{n}}\Big) = \mathsf{b}(\boldsymbol{\mathsf{A}},\mathsf{v})\mathsf{v}, \end{aligned} \tag{2.54}$$

on $\mathcal{S}$. Here, consistent with the convention that $\boldsymbol{\mathsf{n}}$ points into $\mathcal{R}_\beta$, $\llbracket g_\gamma\rrbracket = g_\beta - g_\alpha$. The interface conditions (2.53) and (2.54) are supplemented by the conditions (2.6) of coherency and (2.27) and local equilibrium.

Missing from the foregoing list of equations are the bulk and interfacial moment balances $(2.13)_2$ and $(2.14)_2$, the bulk configurational force balance (2.16), and the tangential component of the interfacial configurational force balance (2.17). Implicit to (2.44), (2.45), and (2.51) is the requirement that the constitutive response functions be properly invariant under superposed rigid motions. Hence, granted (2.44) and (2.51), the bulk and interfacial moment balances $(2.13)_2$ and $(2.14)_2$ are satisfied and may be removed from further consideration. Because it does not appear in the free-energy inequality (2.33), the bulk configurational force $\mathbf{f}$ cannot be determined independently via a constitutive relation. Instead, this force is assigned to ensure satisfaction of the bulk configurational force balance (2.16). That is, $\mathbf{f}$ is given by $\mathbf{f} = -\mathrm{Div}\,\mathbf{C}$. To determine the form of $\mathbf{f}$, we use the constitutive relations (2.41) in the bulk Eshelby relation (2.36) and compute $\mathrm{Div}\,\mathbf{C}$. As a consequence of the bulk deformational force balance (2.52) and the homogeneity of (2.41), it follows that $\mathrm{Div}\,\mathbf{C} = -c\mathrm{Grad}\,u$ and, thus, that $\mathbf{f} = c\mathrm{Grad}\,u$. Hence, $\mathbf{f}$ vanishes when the diffusion potential is uniform. The role of the tangential component $\boldsymbol{\mathsf{f}}_{\mathrm{tan}}$ of the interfacial configurational force $\boldsymbol{\mathsf{f}}$ is analogous to that of $\mathbf{f}$. Being absent from the free-energy inequality (2.38),[4] $\boldsymbol{\mathsf{f}}_{\mathrm{tan}}$ is assigned to ensure satisfaction of the tangential component of the interfacial configurational force balance (2.17). That is, $\boldsymbol{\mathsf{f}}_{\mathrm{tan}}$ is given by $\boldsymbol{\mathsf{f}}_{\mathrm{tan}} = -\boldsymbol{\mathsf{P}}(\llbracket\mathbf{C}\rrbracket\boldsymbol{\mathsf{n}}+\mathrm{Div}_{\mathcal{S}}\boldsymbol{\mathsf{C}})$. To determine the form of $\boldsymbol{\mathsf{f}}_{\mathrm{tan}}$, we use the constitutive relations (2.41) and $(2.48)_{1,2}$ in the bulk and interfacial Eshelby relations (2.36) and (2.17) and

---

[4] For the application under consideration, changes in material structure are limited to those associated with transitions between the collapsed and swelled phases. Constitutively, such transitions are embodied by the relation (2.49) determining f.

compute $[\![\mathsf{C}]\!]\mathsf{n} + \mathrm{Div}_{\mathcal{S}}\mathsf{C}$. As a consequence of the interfacial deformational force balance (2.14) and the homogeneity of $(2.48)_{1,2}$, it follows that $\mathsf{P}([\![\mathsf{C}]\!]\mathsf{n} + \mathrm{Div}_{\mathcal{S}}\mathsf{C}) = \mathbf{0}$ and, thus, that $\mathsf{f}_{\mathrm{tan}} = \mathbf{0}$.

2.8 Boundary conditions

Writing $\boldsymbol{\nu}$ for the unit orientation of $\partial\mathcal{R}$, directed outward from $\mathcal{R}$, we assume that

$$\mathbf{y}|_{(\partial\mathcal{R})_{\mathrm{m}}} = \boldsymbol{\eta} \qquad \text{and} \qquad (\mathbf{S}\boldsymbol{\nu})|_{(\partial\mathcal{R})_{\mathrm{t}}} = \mathbf{s}, \tag{2.55}$$

with $(\partial\mathcal{R})_{\mathrm{m}}$ and $(\partial\mathcal{R})_{\mathrm{t}}$ complementary subsets of $\partial\mathcal{R}$, and that

$$u|_{(\partial\mathcal{R})_{\mathrm{p}}} = \upsilon \qquad \text{and} \qquad (\mathbf{h}\cdot\boldsymbol{\nu})|_{(\partial\mathcal{R})_{\mathrm{f}}} = h, \tag{2.56}$$

with $(\partial\mathcal{R})_{\mathrm{p}}$ and $(\partial\mathcal{R})_{\mathrm{f}}$ complementary subsets of $\partial\mathcal{R}$.

3 Specialization of the theory

Motivated by the experimental observations of Gehrke et al. (1992), we now specialize the theory to situations in which the time scale associated with the motion of the interface is slow with respect to that associated with diffusion in the bulk phases. Following Gurtin and Voorhees (1993), such a theory arises by restricting the Gibbs-energy density in each phase to be linear in u, viz.,

$$\Omega_\gamma(\mathbf{F}, u) = W_\gamma(\mathbf{F}) - c_\gamma u, \tag{3.1}$$

with c_γ constant. Consistent with the intuitive expectation that the solute concentration in the collapsed phase should exceed that in the swelled phase, we assume that

$$0 < c_\alpha < c_\beta < 1. \tag{3.2}$$

In keeping with (2.44), we note that the bulk strain-energy densities W_γ must obey $W_\gamma(\mathbf{F}) = \hat{W}_\gamma(\imath(\mathbf{B}))$.

In addition, we assume that

$$\mathbf{M}_\gamma(\mathbf{F}, u) = m_\gamma \mathbf{I}, \tag{3.3}$$

where m_γ is the constant (scalar) molecular mobility in phase γ and, by (2.43), consistent with

$$m_\gamma > 0. \tag{3.4}$$

Further, for simplicity, we assume that the interfacial free-energy density is constant

$$\tilde{\Psi}(\mathsf{A}) = \sigma, \tag{3.5}$$

so that $\mathsf{S} = \mathbf{0}$, and we neglect transition kinetics by setting

$$\mathsf{b}(\mathsf{A}, \mathsf{v}) = 0. \tag{3.6}$$

Granted the constitutive specializations (3.1) and (3.3), (2.52) yields

$$\left.\begin{aligned} \mathrm{Div}\Big(\frac{\partial W_\gamma(\mathbf{F})}{\partial \mathbf{F}}\Big) &= \mathbf{0}, \\ m_\gamma \mathrm{Div}\,(\mathrm{Grad}\, u) &= 0. \end{aligned}\right\} \tag{3.7}$$

Similarly, granted the constitutive specializations (3.5) and (3.6), (2.53) and (2.54) yield

$$\left.\begin{aligned}\left\llbracket\frac{\partial W_\gamma(\mathbf{F})}{\partial \mathbf{F}}\right\rrbracket\mathsf{n} &= \mathbf{0},\\ \llbracket c_\gamma\rrbracket\mathsf{v} + \llbracket m_\gamma \operatorname{Grad} u\rrbracket\cdot\mathsf{n} &= 0,\\ \llbracket c_\gamma\rrbracket\mathsf{u} = \sigma\mathsf{K} + \mathsf{n}\cdot\left\llbracket W_\gamma(\mathbf{F})\mathbf{I} - \mathbf{F}^{\top}\frac{\partial W_\gamma(\mathbf{F})}{\partial \mathbf{F}}\right\rrbracket&\mathsf{n}.\end{aligned}\right\} \tag{3.8}$$

The interface conditions (3.8) are supplemented by the conditions (2.6) of coherency and (2.27) and local equilibrium.

The only explicit coupling between the fields $\mathbf{y}$ and u evident from (3.7) and (3.8) is through the normal configurational balance $(3.8)_3$.

4 Numerical approximation

Here, we use the hybrid eXtended-Finite-Element/Level-Set Method (XFE/LSM) to discretize the bulk and interfacial equations (3.7) and (3.8), while enforcing the conditions (2.6) and (2.27) of coherency and local chemical equilibrium. Our approach follows upon work of Merle and Dolbow (2002) and Ji et al. (2002) (see Dolbow (1999) for additional details). We begin by deriving an equivalent variational formulation of the governing equations. We then construct an enhanced approximation space for capturing gradient discontinuities across the phase interface. We conclude with a discussion of the solution strategy for the coupled systems of equations.

4.1 Variational formulation

4.1.1 Weak statement of the deformational force balance and coherency

Our variational formulation is non-standard in that the coherency condition (2.6) is enforced weakly using a Lagrange multiplier $\mathbf{p}$. We begin by defining a functional

$$F(\mathbf{y},\mathbf{p}) = \sum_{\gamma=\alpha,\beta}\int\limits_{\mathcal{R}_\gamma} W_\gamma(\mathbf{F})\,dv - \int\limits_{(\partial\mathcal{R})_{\mathrm{t}}} \mathbf{s}\cdot\mathbf{y}\,da - \int\limits_{\mathcal{S}} \mathbf{p}\cdot\llbracket\mathbf{y}\rrbracket\,da. \tag{4.1}$$

The bulk force balance $(3.7)_1$, the interfacial force balance $(3.8)_1$, the coherency condition (2.6), and the traction boundary condition $(2.55)_2$ follow on requiring that F be stationary.

We let $\mathcal{A}_{\mathrm{m}}$ and $\mathcal{L}_{\mathrm{m}}$ denote, respectively, the space of motions and that are sufficiently regular and comply with the Dirichlet conditions $(2.55)_1$ and the space of sufficiently regular Lagrange multipliers.[5] The requirement that F be stationary yields the variational boundary-value-problem: find $\mathbf{y}$ in $\mathcal{A}_{\mathrm{m}}$ and all $\mathbf{p}$ in $\mathcal{L}_{\mathrm{m}}$ such that

$$\left.\begin{aligned}\sum_{\gamma=\alpha,\beta}\int\limits_{\mathcal{R}_\gamma}\frac{\partial W_\gamma(\mathbf{F})}{\partial\mathbf{F}}\cdot\operatorname{Grad}\mathbf{w}\,dv &= \int\limits_{(\partial\mathcal{R})_{\mathrm{t}}}\mathbf{s}\cdot\mathbf{w}\,da + \int\limits_{\mathcal{S}}\mathbf{p}\cdot\llbracket\mathbf{w}\rrbracket\,da,\\ \int\limits_{\mathcal{S}}\mathbf{q}\cdot\llbracket\mathbf{y}\rrbracket\,da &= 0,\end{aligned}\right\} \tag{4.2}$$

for all variations $\mathbf{w}$ of $\mathbf{y}$ and $\mathbf{q}$ of $\mathbf{p}$ belonging to suitable spaces of variations $\mathcal{V}_{\mathrm{m}}$ and $\mathcal{L}_{\mathrm{m}}$.

---

[5] We consider a space of admissible motions that allows for discontinuities across $\mathcal{S}$, even though such discontinuities are not expected in the solution to the strong form of the boundary value problem. Such variational formulations are often termed *hybrid.*

4.1.2 Weak statement of bulk solute balance, interfacial configurational force balance, and local chemical equilibrium

Our next step is also nonstandard. Analogous to our variational treatment of the force balance, we enforce the condition (2.27) of local chemical equilibrium using a scalar-valued Lagrange multiplier k which may jump across the interface.[6] Furthermore, as opposed to formulating a weak statement that imposes the bulk and interfacial solute balances $(3.7)_2$ and $(3.8)_2$, we formulate a weak statement that imposes the bulk solute balance $(3.7)_2$, the interfacial configurational balance $(3.8)_3$, and the condition of local chemical equilibrium. We begin by defining a functional

$$G(u,p)=\sum_{\gamma=\alpha,\beta}\int\limits_{\mathcal{R}_\gamma}\tfrac{1}{2}m_\gamma|\mathrm{Grad}\,u|^2\,dv-\int\limits_{\partial\mathcal{R}_h}hu\,da+\int\limits_{\mathcal{S}}[\![k(\mathsf{u}-u)]\!]\,da. \tag{4.3}$$

The requirement that this functional be stationary implies satisfaction of the bulk solute balance $(3.7)_2$, requires that the interfacial limits $\overset{+}{u}$ and $\overset{-}{u}$ of the diffusion potential coincide and be equal to u (cf. (2.28)), viz.,

$$\overset{+}{u}=\overset{-}{u}=\mathsf{u}, \tag{4.4}$$

and thus ensures satisfaction of the normal configurational force balance $(3.8)_3$ and the condition (2.27) of local chemical equilibrium, while providing identifications,

$$\overset{\pm}{k}=\overline{m_\gamma\overset{\pm}{\mathrm{Grad}}\,u\cdot\mathbf{n}}, \tag{4.5}$$

of the interfacial limits of the Lagrange multiplier with the corresponding interfacial limits of the normal component of the solute flux.

We denote the spaces of sufficiently regular diffusion potentials and Lagrange multipliers by $\mathcal{A}_\mathrm{p}$ and $\mathcal{L}_\mathrm{p}$. The requirement that G be stationary yields the variational boundary-value problem: find u in $\mathcal{A}_\mathrm{p}$ and k in $\mathcal{L}_\mathrm{p}$ such that

$$\left.\begin{aligned}\sum_{\gamma=\alpha,\beta}\int\limits_{\mathcal{R}_\gamma}m_\gamma\mathrm{Grad}\,u\cdot\mathrm{Grad}\,w\,dv&=\int\limits_{(\partial\mathcal{R})_\mathrm{f}}hw\,da-\int\limits_{\mathcal{S}}[\![kw]\!]\,da,\\ \int\limits_{\mathcal{S}}[\![(\mathsf{u}-u)l]\!]\,da&=0,\end{aligned}\right\} \tag{4.6}$$

for all variations w of u and l of k belonging to suitable spaces of variations $\mathcal{V}_\mathrm{p}$ and $\mathcal{L}_\mathrm{p}$.

4.1.3 Interfacial solute balance. Level-set formulation

We have presented variational formulations that lead to weak restatements of all of the equations in (3.7) and (3.8) except the interfacial solute balance $(3.8)_2$. Relying on the expressions (4.5) determining the interfacial limits of the Lagrange multiplier k, we impose $(3.8)_2$ in the strong sense via

$$[\![c_\gamma]\!]\mathsf{v}=-[\![k]\!]. \tag{4.7}$$

We represent the interface as the zero-level set

$$\mathcal{S}(t)=\{\mathbf{x}:\zeta(\mathbf{x},t)=0\} \tag{4.8}$$

---

[6] In practice, two independent Lagrange multipliers are employed and these are indeterminate away from the interface. For the sake of convenience, we refer to these here as separate limiting values of a single bulk field k.

of a function ζ and, following Osher and Sethian (1988), replace (4.7) with the evolution equation

$$\dot{\zeta} + v|\mathrm{Grad}\,\zeta| = 0, \tag{4.9}$$

where the extension velocity v is constrained to obey

$$v|_{\zeta=0} = \mathsf{v} = -\frac{k}{[\![c_\gamma]\!]} \tag{4.10}$$

Further, we require that

$$\mathrm{Grad}\,v\cdot\mathrm{Grad}\,\zeta = 0, \tag{4.11}$$

which is both necessary and sufficient (Sethian, 1996) to ensure that ζ is the signed distance from the interface $\mathcal{S}$. Since ζ is defined throughout $\mathcal{R}$, (4.9) is an evolution equation over $\mathcal{R}$.

4.2 Discretization with the XFE/LSM

4.2.1 Approximation for the motion $\mathbf{y}$

Finite-element computations entail the projection of the solution space $\mathcal{A}_\mathrm{m}$ and the associated space $\mathcal{V}_\mathrm{m}$ of variations onto finite-dimensional subspaces $\mathcal{A}^h_\mathrm{m}$ and $\mathcal{V}^h_\mathrm{m}$, and similarly for the Lagrange multipliers. The Galerkin approximation of the variational boundary-value problem stated in Section 4.1.1 reads: find $\mathbf{y}^h$ in $\mathcal{A}^h_\mathrm{m}$ and $\mathbf{p}^h$ in $\mathcal{L}^h_\mathrm{m}$ such that

$$\left.\begin{aligned} \sum_{\gamma=\alpha,\beta} \int\limits_{\mathcal{R}_\gamma} \frac{\partial W_\gamma(\mathbf{F}^h)}{\partial \mathbf{F}^h}\cdot\mathrm{Grad}\,\mathbf{w}^h\,dv &= \int\limits_{(\partial\mathcal{R})_\mathrm{t}} \mathbf{s}\cdot\mathbf{w}^h\,da + \int\limits_{\mathcal{S}} \mathbf{p}^h\cdot[\![\mathbf{w}^h]\!]\,da, \\ \int\limits_{\mathcal{S}} \mathbf{q}^h\cdot[\![\mathbf{y}^h]\!]\,da &= 0, \end{aligned}\right\} \tag{4.12}$$

for all variations $\mathbf{w}^h$ of $\mathbf{y}^h$ and $\mathbf{q}^h$ of $\mathbf{p}^h$ belonging to $\mathcal{V}^h_\mathrm{m}$ and $\mathcal{L}^h_\mathrm{m}$.

We use M to denote the total number of elements in the mesh and consider a regular finite-element-triangulation $\mathcal{Q}^h = \cup_{e=1}^M \mathcal{Q}_e$, with $\mathcal{Q}^h = \mathcal{R}$ but with element edges chosen, generally, to be independent of the interface geometry. Letting $P^j(\mathcal{Q}_e)$ denote the space of complete polynomials of order less than or equal to j over element $\mathcal{Q}_e$, we introduce

$$\{\phi_i \in C^0(\mathcal{Q}^h) : \phi_i|\mathcal{Q}_e \in P^j(\mathcal{Q}_e)\}, \tag{4.13}$$

where ϕ_i, $i = 1, 2, \dots,$ are the nodal shape functions. We next consider the set of overlapping subdomains $\{\omega_i\}$ defining the support of each nodal shape function and an enrichment function g that possesses desirable approximation properties in the vicinity of the interface. The approximation for the deformation is given by

$$\mathbf{y}^h(\mathbf{x},t) = \underbrace{\sum_{i\in I} \mathbf{c}_i(t)\phi_i(\boldsymbol{\xi}(\mathbf{x}))}_{\text{classical approximation}} + \underbrace{\sum_{j\in J} \mathbf{e}_j(t)\phi_j(\boldsymbol{\xi}(\mathbf{x}))g(\mathbf{x},t)}_{\text{enrichment}} \tag{4.14}$$

where $\boldsymbol{\xi}$ are the local element coordinates. In the above, I denotes the set of all nodes in the mesh and $J = \{j \in I : \omega_j \cap \mathcal{S} \neq \emptyset\}$ the set of nodes that form a partition of unity for g (Melenk and Babuška, 1996).

As shown by Ji (2001), g must meet specific conditions to ensure optimal rates of convergence in the energy norm and the local quantities of interest at the interface, such as the jump $[\![m_\gamma \mathrm{Grad}\, u]\!]$ appearing in $(3.8)_2$. Here, we use the characteristic function for the β phase, in which case

$$g(\mathbf{x}, t) = \chi_\beta(\mathbf{x}, t) = \begin{cases} 0 & \mathbf{x} \in \mathcal{R}_\alpha(t), \\ 1 & \mathbf{x} \in \mathcal{R}_\beta(t). \end{cases} \tag{4.15}$$

As the discontinuity of χ_β coincides with the phase interface, the choice $g = \chi_\beta$ provides a mechanism for the approximation (4.14) to represent the geometry of the interface independent of the element boundaries.[7] Furthermore, as the interface evolves, we update the enrichment function and the set J; no remeshing is performed.

With the preceding definitions, we introduce a set

$$\{\Phi_r\}_{r=1}^{N} = \{\phi_i\}_{i=1}^{N_I} \cup \{\phi_j \chi_\beta\}_{j=1}^{N_J}, \tag{4.16}$$

of linearly independent functions Φ_r; this set forms a basis for $\mathcal{A}_{\mathrm{m}}^h$, where N_I and N_J denote, respectively, the number of elements in the sets I and J and $N = N_I + N_J$. We then represent $\mathcal{A}_{\mathrm{m}}^h$ as

$$\mathcal{A}_{\mathrm{m}}^h = \mathrm{span}\{\Phi_r\}_{r=1}^{N}. \tag{4.17}$$

We employ a Bubnov–Galerkin approximation and use this same set of functions to construct $\mathcal{V}_{\mathrm{m}}^h$.[8]

The Lagrange multipliers are approximated by polynomial functions defined on the element interiors. Specifically,

$$\mathcal{L}_{\mathrm{p}}^h = \mathrm{span}\{\lambda_i\}_{i=1}^{N_l}, \qquad \text{with} \qquad \{\lambda_i \in P^k(\mathcal{S}_e)\},$$

where $\mathcal{S}_e$ denotes the intersection of the interface with the element domain $\mathcal{Q}_e$. So, the approximation for the Lagrange multipliers is written as a linear combination

$$\mathbf{p}^h(\mathbf{x}, t) = \sum_i \mathbf{p}_i(t) \lambda_i(\mathbf{x}) \tag{4.18}$$

of these functions. Details of the construction can be found in Dolbow et al. (2001) and Ji et al. (2002). A similar approximation is employed for the variations $\mathbf{q}^h$.

Substitution of the above and (4.14) into (4.12) results in a nonlinear system of equations in $\{\mathbf{c}_i, \mathbf{e}_j, \mathbf{p}_i\}$. We employ the standard Newton–Raphson procedure and solve the above with a sequence of linearized problems. These take the form

$$\mathbf{K}_f^{(n)} \Delta \mathbf{d}_f = \mathbf{r}^{(n)}, \tag{4.19}$$

with $\mathbf{K}_f^n$ the tangent stiffness matrix at iteration n, $\mathbf{r}^n$ the residual vector, and $\Delta\mathbf{d}_f$ the vector gathering the incremental degrees of freedom $\Delta\mathbf{c}_i$, $\Delta\mathbf{e}_j$, and $\Delta\mathbf{p}_i$. After solving the above, the solution is updated by $\mathbf{c}_i^{n+1} = \mathbf{c}_i^n + \Delta\mathbf{c}_i$, $\mathbf{e}_j^{n+1} = \mathbf{e}_j^n + \Delta\mathbf{e}_j$. The construction of the tangent stiffness matrix and residual vector requires the accurate integration of terms containing the classical and enriched basis functions over the element subdomains. The standard element-based quadrature routines are modified for those elements wherein the functions are discontinuous. Details for these modifications are provided by Dolbow et al. (2000).

---

[7] Similar approaches have been employed by Krongauz and Belytschko (1998) and Sukumar et al. (2001). However, these approaches use continuous enrichment functions.

[8] The construction of $\mathcal{V}_{\mathrm{m}}^h$ only employs those functions Φ_k which vanish on the Dirichlet boundary $(\partial\mathcal{R})_{\mathrm{m}}$.

4.2.2 Approximation for the diffusion potential u

The Galerkin approximation to variational boundary-value problem stated in Section 4.1.2 reads: find u^h in $\mathcal{A}^h_{\mathrm{p}}$ and k^h in $\mathcal{L}^h_{\mathrm{p}}$ such that

$$\left.\begin{aligned}
\int\limits_{\mathcal{R}} m_\gamma \operatorname{Grad} u^h \cdot \operatorname{Grad} w^h \, dv &= \int\limits_{(\partial\mathcal{R})_{\mathrm{f}}} h w^h \, da - \int\limits_{\mathcal{S}} [\![k^h w^h]\!] \, da, \\
\int\limits_{\mathcal{S}} [\![(\mathsf{u} - u^h) l^h]\!] \, da &= 0,
\end{aligned}\right\} \tag{4.20}$$

for all variations w^h of u^h and l^h and k^h belonging to $\mathcal{V}^h_{\mathrm{p}}$ and $\mathcal{L}^h_{\mathrm{p}}$.

The approximation for the diffusion potential takes a form,

$$u^h(\mathbf{x}, t) = \sum_{i \in I} a_i(t) \phi_i(\boldsymbol{\xi}(\mathbf{x})) + \sum_{j \in J} b_j(t) \phi_j(\boldsymbol{\xi}(\mathbf{x})) \chi_\beta(\mathbf{x}, t), \tag{4.21}$$

in which $\{\phi_i\}$ is the set of nodal shape functions used in the approximation for the motion. The above may be viewed as the scalar analog to (4.14). Here, the enrichment allows the approximation u^h to represent the arbitrary gradient discontinuities in the diffusion potential across the interface. The approximation for the Lagrange multiplier k takes a scalar form analogous to (4.18), viz.,

$$\overset{\pm}{k}{}^h(\mathbf{x}, t) = \sum_i \overset{\pm}{k}_i(t) \lambda_i(\mathbf{x}). \tag{4.22}$$

We again adopt a Bubnov–Galerkin approximation and write approximations for the variations w^h and l^h in the forms similiar to (4.21) and (4.22), respectively. Upon substituting the approximations into the discrete weak form (4.20) and invoking the arbitrariness of the variations, we obtain a linear system of equations

$$\mathbf{K}_u \mathbf{d}_u = \mathbf{f}_u, \tag{4.23}$$

where $\mathbf{d}_u$ gathers the degrees of freedom a_i, b_j, and k_i.

4.2.3 Staggered solution strategy

Equation (4.9) is solved using a finite-difference stencil independent of the finite-element mesh. The technique employs standard upwinding algorithms taken from those developed for the solution of hyperbolic conservation laws. The details of the approach are given by in Chopp (2001) and Ji et al. (2002).

We now describe the solution strategy for the full system. Assuming that all fields and the geometry of the interface $\mathcal{S}$ are known at some time t^n, the first step it to advect the level-set function through the system (4.9) and, thereby, to obtain the position of the interface at t^{n+1}. The nonlinear system (4.19) is then solved and the fields are post-processed to obtain the interfacial diffusion potential through the normal configurational force balance (3.8). Finally, the approximation for the diffusion potential is obtained by solving (4.23), completing the determination of all bulk fields at time t^{n+1}. The solution of (4.23) also yields the approximation for the Lagrange multipliers. These are used at time step t^{n+1} to evaluate the velocity of the interface through (4.7). The above process is then repeated. This strategy is exact and does not require iteration within a time step.

The feasibility of the above solution strategy rests on the constitutive specializations described in Section 3, which lead to equations in which the coupling between the deformation and diffusion potential is solely through the interfacial conditions. In the more general equations (2.52) and (2.53), the strong coupling of the bulk fields would require an alternative strategy.

5 Application: Swelling of a spherical specimen

5.1 Constitutive specialization

To model the deformational response of the bulk phases, we now specify a bulk strain-energy density W_γ for each phase γ. For simplicity, we assume that

$$W_\gamma(\mathbf{F}) = \frac{\mu_\gamma}{2}(|\mathbf{F}|^2 - 2J_\gamma^{\frac{2}{3}} \log\det(J_\gamma^{-\frac{1}{3}}\mathbf{F}) - 3J_\gamma^{\frac{2}{3}}) + \frac{\lambda_\gamma J_\gamma^{\frac{2}{3}}}{4}\big((\det(J_\gamma^{-\frac{1}{3}}\mathbf{F}) - 1)^2 + \log^2\det(J_\gamma^{-\frac{1}{3}}\mathbf{F})\big) + J_\gamma^{\frac{2}{3}} w_\gamma, \tag{5.1}$$

with $\mu_\gamma > 0$ and $\lambda_\gamma > 0$ mechanical moduli for phase γ and w_γ constant.

To illustrate some features of this choice, we consider pure dilatations $\mathbf{F} = \xi J_\gamma^{1/3}\mathbf{I}$, with $\xi > 0$, and introduce

$$\mathcal{W}_\gamma(\xi) = W_\gamma(\xi J_\gamma^{\frac{1}{3}}\mathbf{I}). \tag{5.2}$$

Then, for all admissible ξ, direct calculations show that, by the assumed positivity of μ_γ and λ_γ,

$$\mathcal{W}_\gamma(\xi) \ge w_\gamma J_\gamma^{\frac{2}{3}} \qquad \text{and} \qquad \frac{d^2\mathcal{W}_\gamma(\xi)}{d\xi^2} \ge 0. \tag{5.3}$$

Hence, when restricted to pure dilatations, W_γ is bounded below by $J_\gamma^{2/3} w_\gamma$ and is convex. Further, since

$$\min_{\xi>0} \mathcal{W}_\gamma(\xi) = \mathcal{W}_\gamma(1) = w_\gamma J_\gamma^{\frac{2}{3}}, \tag{5.4}$$

J_γ is the energetically-preferred dilatation for phase γ.

A sense of the relative importance of the moduli μ_γ and λ_γ is given by considering the scaled difference

$$\frac{\mathcal{W}_\gamma(\xi) - w_\gamma J_\gamma^{\frac{2}{3}}}{\mu_\gamma J_\gamma^{\frac{2}{3}}} \tag{5.5}$$

for a range of the dimensionless parameter $\mu_\gamma/\lambda_\gamma$ (Figure 2).

Since a strain-energy density can be determined only up to an arbitrary additive constant, it is the difference

$$[\![J_\gamma^{\frac{1}{3}} w_\gamma]\!] = J_\beta^{\frac{1}{3}} w_\beta - J_\alpha^{\frac{1}{3}} w_\alpha \tag{5.6}$$

rather than the individual values $J_\gamma^{\frac{1}{3}} w_\gamma$ that are important in what follows.

Next, an easy calculation shows that

$$\frac{\partial W_\gamma(\mathbf{F})}{\partial \mathbf{F}} = \mu_\gamma(\mathbf{F} - J_\gamma^{\frac{2}{3}}\mathbf{F}^{-\top}) + \frac{\lambda_\gamma J_\gamma^{\frac{2}{3}}}{2}\Big((\det(J_\gamma^{-\frac{1}{3}}\mathbf{F}) - 1)\det(J_\gamma^{-\frac{1}{3}}\mathbf{F}) + \log\det(J_\gamma^{-\frac{1}{3}}\mathbf{F})\Big)\mathbf{F}^{-\top}. \tag{5.7}$$

Thus,

$$\frac{\partial W_\gamma(\mathbf{F})}{\partial \mathbf{F}}\Big|_{\mathbf{F}=J_\gamma^{\frac{1}{3}}\mathbf{I}} = \mathbf{0}, \tag{5.8}$$

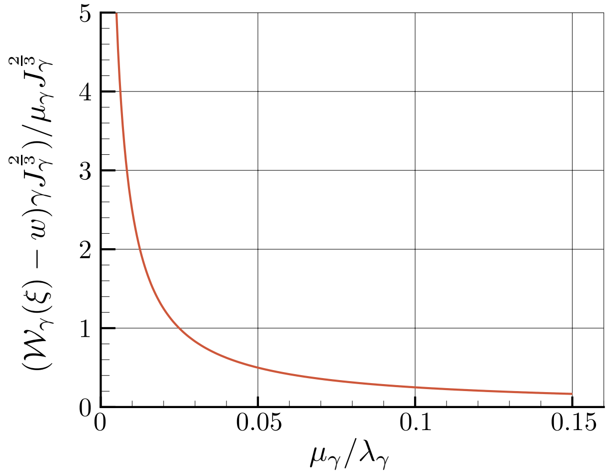

Figure 2: Relative importance of μ_γ and λ_γ to bulk strain-energy density.

and we conclude that phase γ is stress-free at the energetically-preferred dilatation $\mathbf{F} = J_\gamma^{1/3}\mathbf{I}$.

Further, a lengthy calculation yields

$$\begin{aligned}\frac{\partial^2 W_\gamma(\mathbf{F})}{\partial \mathbf{F}^2} &= \mu_\gamma(\mathbf{I}\boxtimes\mathbf{I} + J_\gamma^{\frac{2}{3}}\mathbb{T}(\mathbf{F}^{-\top}\boxtimes\mathbf{F}^{-\top}))\\ &\quad - \frac{\lambda_\gamma J_\gamma^{\frac{2}{3}}}{2}((\det(J_\gamma^{-\frac{1}{3}}\mathbf{F}) - 1)\det(J_\gamma^{-\frac{1}{3}}\mathbf{F})) + \log\det(J_\gamma^{-\frac{1}{3}}\mathbf{F}))\mathbb{T}(\mathbf{F}^{-\top}\boxtimes\mathbf{F}^{-\top}))\\ &\quad + \frac{\lambda_\gamma J_\gamma^{\frac{2}{3}}}{2}((2\det(J_\gamma^{-\frac{1}{3}}\mathbf{F}) - 1)\det(J_\gamma^{-\frac{1}{3}}\mathbf{F}) + 1)\mathbf{F}^{-\top}\otimes\mathbf{F}^{-\top}, \end{aligned} \tag{5.9}$$

where $\mathbf{H}\boxtimes\mathbf{K}$, $\mathbb{T}$, $\mathbf{H}\otimes\mathbf{K}$ are the fourth-order tensors defined (Del Piero, 1979) so that, for any second-order tensor $\mathbf{A}$, $(\mathbf{H}\boxtimes\mathbf{K})\mathbf{A} = \mathbf{H}\mathbf{A}\mathbf{K}^\top$, $\mathbb{T}\mathbf{A} = \mathbf{A}^\top$, and $(\mathbf{H}\otimes\mathbf{K})\mathbf{A} = (\mathbf{K}\cdot\mathbf{A})\mathbf{H}$. An immediate consequence of (5.9) is that

$$\frac{\partial^2 W_\gamma(\mathbf{F})}{\partial \mathbf{F}^2}\Big|_{\mathbf{F}=J_\gamma^{\frac{1}{3}}\mathbf{I}} = \mu_\gamma(\mathbf{I}\boxtimes\mathbf{I} + \mathbb{T}(\mathbf{I}\boxtimes\mathbf{I})) + \lambda_\gamma\mathbf{I}\otimes\mathbf{I}. \tag{5.10}$$

Thus, μ_γ and λ_γ correspond to conventional shear and Lamé moduli for infinitesimal deviations from the stress-free state in phase γ. A more far-reaching consequence of (5.9) is that, by the assumed positivity of μ_γ and λ_γ,

$$\begin{aligned}\mathbf{a}\otimes\mathbf{b}\cdot\Big(\frac{\partial^2 W_\gamma(\mathbf{F})}{\partial \mathbf{F}^2}\mathbf{a}\otimes\mathbf{b}\Big) &= \mu_\gamma(|\mathbf{a}|^2|\mathbf{b}|^2 + 2J_\gamma^{\frac{2}{3}}(\mathbf{F}^{-1}\mathbf{a}\cdot\mathbf{b})^2)\\ &\quad + \frac{\lambda_\gamma J_\gamma^{\frac{2}{3}}}{2}\Big(1 + \Big(\frac{\det\mathbf{F}}{J_\gamma}\Big)^2 - \frac{1}{2}\log\Big(\frac{\det\mathbf{F}}{J_\gamma}\Big)\Big)(\mathbf{F}^{-1}\mathbf{a}\cdot\mathbf{b})^2 > 0. \end{aligned} \tag{5.11}$$

Thus, the strain-energy density of each phase is rank-one convex.

Without loss of generality, we assume that

$$J_\beta = 1. \tag{5.12}$$

Then, since α is the swelled phase, we must necessarily have

$$J_\alpha > 1. \tag{5.13}$$

5.2 Kinematical specialization

We consider the problem of a traction-free specimen suspended in a solvent-rich reservoir of solution with uniform diffusion potential. We assume that, in the reference configuration, the specimen occupies the spherical region

$$\mathcal{R} = \{\mathbf{x} : |\mathbf{x}| \leq R\}. \tag{5.14}$$

Writing

$$\mathbf{e} = \frac{\mathbf{x}}{|\mathbf{x}|}, \tag{5.15}$$

the requirement that the specimen be traction-free yields

$$\mathbf{S}\mathbf{e}|_{\partial\mathcal{R}} = \mathbf{0}. \tag{5.16}$$

Further, writing $U(t)$ for the value of the diffusion potential of the reservoir at time t, we have

$$u|_{\partial\mathcal{R}} = U. \tag{5.17}$$

We restrict attention to circumstances in which the deformation and the diffusion potential depend at most on radial position $r = |\mathbf{x}|$ and time t, viz.,

$$\mathbf{y}(\mathbf{x}, t) = y(r, t)\mathbf{e} \qquad \text{and} \qquad u(\mathbf{x}, t) = u(r, t). \tag{5.18}$$

Consistent with these assumptions, we suppose that the interface is concentric, and write

$$\mathcal{S}(t) = \{\mathbf{x} : |\mathbf{x}| = \mathsf{s}(t)\} \tag{5.19}$$

for its position at time t. Anticipating that swelling should proceed from the boundary inwards towards the center of the specimen,

$$\mathsf{n} = -\mathbf{e}, \qquad \mathsf{K} = \mathrm{Grad}_{\mathcal{S}}\mathsf{n} = -\frac{2}{\mathsf{s}}, \qquad \text{and} \qquad \mathsf{v} = -\dot{\mathsf{s}}. \tag{5.20}$$

We use g' to denote the partial derivative of a field g with respect to r. Thus, by $(5.18)_1$, the deformation gradient has the particular form

$$\mathbf{F}(r, t) = y'(r, t)\mathbf{e}\otimes\mathbf{e} + \frac{y(r, t)}{r}(\mathbf{I} - \mathbf{e}\otimes\mathbf{e}) \tag{5.21}$$

and the associated Jacobian is given by

$$J(r, t) = \det\mathbf{F}(r, t) = \frac{y^2(r, t)y'(r, t)}{r^2} > 0. \tag{5.22}$$

Since $\det\mathbf{F} > 0$, it follows that y must obey

$$y(r, t) \geq 0 \qquad \text{and} \qquad y'(r, t) > 0, \tag{5.23}$$

for $0 < r \leq R$, as well as

$$y(r, t) \sim r \quad \text{and} \quad y'(r, t) \sim 1 \quad \text{as} \quad r \to 0. \tag{5.24}$$

5.3 Reduced governing equations

5.3.1 Bulk equations

In view of (5.7), (5.21), and (5.22),

$$\frac{\partial W_\gamma(\mathbf{F})}{\partial \mathbf{F}} = S_\parallel \mathbf{e}\otimes\mathbf{e} + S_\perp(\mathbf{I} - \mathbf{e}\otimes\mathbf{e}), \tag{5.25}$$

with

$$S_\parallel(r,t) = \mu_\gamma\Big(y'(r,t) - \frac{J_\gamma^{\frac{2}{3}}}{y'(r,t)}\Big) + \frac{\lambda_\gamma J_\gamma^{\frac{2}{3}} D(r,t)}{2y'(r,t)} \tag{5.26}$$

and

$$S_\perp(r,t) = \mu_\gamma\Big(\frac{y(r,t)}{r} - \frac{J_\gamma^{\frac{2}{3}} r}{y(r,t)}\Big) + \frac{\lambda_\gamma J_\gamma^{\frac{2}{3}} r D(r,t)}{2y(r,t)} \tag{5.27}$$

the components of radial and hoop stress, and (cf. (5.22))

$$D(r,t) = \frac{J(r,t)}{J_\gamma}\Big(\frac{J(r,t)}{J_\gamma} - 1\Big) + \log\Big(\frac{J(r,t)}{J_\gamma}\Big). \tag{5.28}$$

Thus, the deformational force balance $(3.7)_1$ reduces to the scalar equation $(r^2 S_\parallel(r,t))' = 2rS_\perp(r,t)$, which, by (5.26) and (5.27), can be written as

$$\begin{aligned}\Big(\mu_\gamma r^2\Big(y'(r,t) - \frac{J_\gamma^{\frac{2}{3}}}{y'(r,t)}\Big) + \frac{\lambda_\gamma J_\gamma^{\frac{2}{3}} r^2 D(r,t)}{2y'(r,t)}\Big)'&\\ = 2\mu_\gamma\Big(y(r,t) - \frac{J_\gamma^{\frac{2}{3}} r^2}{y(r,t)}\Big) + \frac{\lambda_\gamma J_\gamma^{\frac{2}{3}} r^2 D(r,t)}{y(r,t)}.&\end{aligned} \tag{5.29}$$

Similarly, by $(5.18)_2$, the solute balance $(3.7)_2$ simplifies to

$$m_\gamma\big(r^2 u'(r,t)\big)' = 0. \tag{5.30}$$

5.3.2 Interfacial equations

On appealing to (5.25) and $(5.20)_1$, the deformational force balance $(3.8)_1$ reduces to the scalar equation $[\![S_\parallel]\!] = 0$, which, by (5.26), can be written as

$$\Big[\!\!\Big[\mu_\gamma\Big(y'(\mathsf{s}(t),t) - \frac{J_\gamma^{\frac{2}{3}}}{y'(\mathsf{s}(t),t)}\Big) + \frac{\lambda_\gamma J_\gamma^{\frac{2}{3}} D(\mathsf{s}(t),t)}{2y'(\mathsf{s}(t),t)}\Big]\!\!\Big] = 0. \tag{5.31}$$

Similarly, by $(5.18)_2$ and $(5.20)_{1,3}$, the solute balance $(3.8)_2$ simplifies to

$$\dot{\mathsf{s}}(t) = -\frac{[\![m_\gamma u'(\mathsf{s}(t),t)]\!]}{[\![c_\gamma]\!]}. \tag{5.32}$$

Finally, by (5.1), (5.21), (5.25), (5.26), (5.27), and (5.20), the normal configurational force balance (3.8) becomes

$$\begin{aligned}[\![c_\gamma]\!]\mathsf{u}(t) = -\frac{2\sigma}{\mathsf{s}(t)} - \frac{1}{2}\Big[\!\!\Big[\mu_\gamma\Big((y'(\mathsf{s}(t),t))^2 + \frac{2y^2(\mathsf{s}(t),t)}{\mathsf{s}^2(t)} + 2J_\gamma^{\frac{2}{3}}\log\Big(\frac{J(\mathsf{s}(t),t)}{J_\gamma}\Big) - 3J_\gamma^{\frac{2}{3}}\Big)\Big]\!\!\Big]&\\ + \frac{1}{4}\Big[\!\!\Big[\lambda_\gamma J_\gamma^{\frac{2}{3}}\Big(\Big(\frac{J(\mathsf{s}(t),t)}{J_\gamma} - 1\Big)^2 + \log^2\Big(\frac{J(\mathsf{s}(t),t)}{J_\gamma}\Big) - 6D(\mathsf{s}(t),t)\Big)\Big]\!\!\Big] + [\![J_\gamma^{\frac{2}{3}} w_\gamma]\!].&\end{aligned} \tag{5.33}$$

In view of (5.18), the conditions (2.6) and (2.27) of coherency and local equilibrium hold if and only if

$$[\![y(\mathsf{s}(t),t)]\!]=0 \qquad \text{and} \qquad [\![u(\mathsf{s}(t),t)]\!]=0. \tag{5.34}$$

5.3.3 Boundary conditions

The asymptotic restriction (5.24) yields the condition

$$y(0,t)=0 \tag{5.35}$$

at the center of the specimen. By (5.25), the traction-free condition (5.16) reduces to

$$\mu_\alpha\Big(y'(R,t)-\frac{J_\alpha^{\frac{2}{3}}}{y'(R,t)}\Big)+\frac{\lambda_\alpha J_\alpha^{\frac{2}{3}}J(R,t)}{2y'(R,t)}=0. \tag{5.36}$$

The requirement that u be radially-symmetric requires that

$$u'(0,t)=0. \tag{5.37}$$

By $(5.18)_2$, (5.17) becomes

$$u(R,t)=U(t). \tag{5.38}$$

5.3.4 Initial condition

We suppose that the position of the interface is given initially, so that

$$\mathsf{s}(0)=\mathsf{s}_0, \quad \text{with } 0\le \mathsf{s}_0\le R. \tag{5.39}$$

5.4 Analytical observations

Equations (5.29)–(5.39) form an initial-boundary-value problem for determining the bulk deformation y, the bulk diffusion potential u, the interfacial position s, and the interfacial diffusion potential u (with the understanding that $u(\mathsf{s}(t),t)=\mathsf{u}(t)$ for each time t).

If s is treated as given, the bulk and interfacial deformational force balances (5.29) and (5.31), the condition $(5.34)_1$ of coherency, and the boundary conditions (5.35) and (5.36) form a problem that might, in principle, be solved to determine y parametrically in terms of s and the parameters μ_γ, λ_γ, and J_γ. Particular (time-independent) solutions which can be easily verified are

$$y(r)=J_\alpha^{\frac{1}{3}}r, \tag{5.40}$$

corresponding to a specimen which is completely swelled ($\mathsf{s}=0$), and

$$y(r)=J_\beta^{\frac{1}{3}}r, \tag{5.41}$$

corresponding to a specimen which is fully collapsed ($\mathsf{s}=R$). However, for $0<\mathsf{s}<R$, we have not been able to determine y in closed form.

Nevertheless, the bulk solute balance (5.30), the condition $(5.34)_2$ of local chemical equilibrium, and the boundary conditions (5.37) and (5.38) can be solved easily to obtain an expression

$$u(r,t)=\begin{cases}\mathsf{u}(t), & 0<r\le \mathsf{s}(t),\\[2ex] U(t)-\dfrac{\mathsf{s}(t)(U(t)-\mathsf{u}(t))}{R-\mathsf{s}(t)}\Big(\dfrac{R}{r}-1\Big), & \mathsf{s}(t)\le r<R,\end{cases} \tag{5.42}$$

for u in terms of s, u, and the diffusion potential U in the reservoir. This expression shows that, at each time t, the diffusion potential of the collapsed phase is uniform and equal to the interfacial diffusion potential $\mathsf{u}(t)$. Further, unless $U(t) = \mathsf{u}(t)$, (5.42) shows that the diffusion potential of the swelled phase varies monotonically with r—decreasing or increasing from the boundary value $U(t)$ to the interfacial value $\mathsf{u}(t)$ when $\mathsf{u}(t) < U(t)$ and $\mathsf{u}(t) > U(t)$, respectively.

Not covered by (5.42) are the (time-independent) states of complete swelling ($\mathsf{s} = 0$) and collapse ($\mathsf{s} = R$) corresponding to fields y of the forms (5.40) and (5.41), respectively. In both of these cases, (5.42) is replaced by the (time-independent) expression

$$u(r) = U. \tag{5.43}$$

It follows that completely swelled and collapsed states can only occur if the diffusion potential of the specimen is uniform and equal to that of the reservior.

As a simple consequence of (5.42), we may rewrite the interfacial solute balance (5.32) in the form

$$\dot{\mathsf{s}}(t) = -\frac{m_\alpha}{[\![c_\gamma]\!]}\frac{R(U(t) - \mathsf{u}(t))}{\mathsf{s}(t)(R - \mathsf{s}(t))}. \tag{5.44}$$

Together with the initial condition (5.39), (5.44) yields an initial-value problem for s.[9] At any time t, the instantaneous kinetic response of the gel can be characterized by the velocity $\dot{\mathsf{s}}$ of the interface. Bearing in mind (3.2), (3.4), and (5.44),

$$\dot{\mathsf{s}}(t) \begin{cases} < 0 & \text{if } U(t) > \mathsf{u}(t), \\ = 0 & \text{if } U(t) = \mathsf{u}(t), \\ > 0 & \text{if } U(t) < \mathsf{u}(t). \end{cases} \tag{5.45}$$

Hence, whether the specimen swells or shrinks at an instant t is dictated entirely by the difference between the diffusion potential $U(t)$ of the reservoir and the diffusion potential $\mathsf{u}(t)$ in the collapsed phase. When $\mathsf{u}(t) < U(t)$, the interface moves toward the center of the specimen, which increases in volume as the swelled phase grows at the expense of the collapsed phase. When $\mathsf{u}(t) = U(t)$, the diffusion potential is uniform and the volumes occupied by the phases are fixed. When $\mathsf{u}(t) > U(t)$, the interface moves toward the boundary of the specimen, which decreases in volume as the collapsed phase grows at the expense of the swelled phase.

Returning to (5.44), we note that, provided the time-dependence of the difference $U - \mathsf{u}$ is weak in the sense that

$$U(t) - \mathsf{u}(t) \approx U_0, \tag{5.46}$$

with U_0 constant, then, bearing in mind the initial condition (5.39), the differential equation (5.44) can be integrated in closed form to yield s. In the special case where the specimen is initially collapsed, this expression predicts that the time required for complete swelling of the specimen is finite and given by

$$\tau = \frac{[\![c_\gamma]\!]R^2}{6m_\alpha U_0}. \tag{5.47}$$

Despite the unrealistic nature of the assumption (5.46), the prediction (5.47) of swelling time concurs with experimental observations, which indicate that the time required for complete swelling of a collapsed specimen scales with the square of the initial radius of the specimen (Tanaka et al., 1985; Matsuo and Tanaka, 1989)

---

[9] Using the normal configurational force balance (5.33) in (5.44) leads to an alternative version of the interfacial solute balance which, granted knowledge of y constitutes a nonlinear differential equation for s. For brevity, we do not reproduce this equation here.

Property	Normalization	Collapsed phase (β)	Swelled phase (α)
c_γ	c_γ	0.2	0.1
m_γ	$\dfrac{m_\gamma\, T}{R^2(c_\beta - c_\alpha)\Theta}$	0.001	0.002
σ	$\dfrac{\sigma}{R(c_\beta - c_\alpha)}$	0.01	0.01
μ_γ	$\dfrac{\mu_\gamma}{(c_\beta - c_\alpha)\Theta}$	200.0	100.0
λ_γ	$\dfrac{\lambda_\gamma}{(c_\beta - c_\alpha)\Theta}$	10000	5000
J_γ	J_γ	1.0	10.0
w_γ	$\dfrac{w_\gamma}{(c_\beta - c_\alpha)\Theta}$	0.0	20.0

Table 1: Baseline material properties and parameters used in the parametric studies. Normalized quantities are provided based on a gel with radius $R = 1.00$ cm, characteristic swelling time $T = 100$ s, and characteristic diffusion potential $\Theta = 1.00$ J.

5.5 Numerical results

In view of (5.42) and (5.44), the initial-boundary-value problem (5.29)–(5.39) is equivalent to a reduced problem for y, u, and s and consisting of (5.29), (5.31), (5.33), $(5.34)_1$, (5.35), (5.36), and (5.39). This reduction occurs solely due to the radial symmetry of the problem at hand. Under more general circumstances, (5.42) would replaced by an integral representation for the diffusion potential and the corresponding reduced problem would be nonlocal. With a view to studying problems involving specimens of arbitrary geometry, we use the numerical method described in Section 4.2 to study the initial-boundary-value problem (5.29)–(5.39).

In the sections that follow, we conduct studies that examine how particular material parameters in the model influence the numerical predictions. The baseline quantities for these studies, considering a gel with an initial radius of $R = 1.00$ cm, a characteristic swelling time of $T = 100$ s, and a characteristic diffusion potential of $\Theta = 1.00$ J, are provided in Table 1. We begin by investigating static solutions that result on fixing the position of the interface along with the diffusion potential of the reservoir. We then study problems in which the interface is allowed to evolve and equilibrate under the influence of a given diffusion potential of the reservoir. Finally, we consider the response of the specimen to cyclic changes of the diffusion potential of the reservoir.

5.5.1 Static two-phase states

Assuming that the value U of the diffusion potential of the reservoir is time-independent, we consider the artificial problem of constructing solutions for given fixed positions s of the interface. In this case, the problem reduces to determining t-independent y and u

from (5.29)–(5.38), excepting (5.32).

We first examine the influence of the preferred dilation $J_\alpha > 1$ of the swelled phase and the mechanical moduli μ_γ and λ_γ on the net volumetric expansion of the specimen. To quantify this change, we introduce the macroscopic swelling ratio

$$Q = \frac{y^3(R)}{R^3}. \tag{5.48}$$

An upper bound $Q_{\max}$ for this ratio is provided by the completely-swelled state (5.40), which yields $Q_{\max} = J_\alpha$. We note that this bound is independent of the mechanical moduli μ_γ and λ_γ.

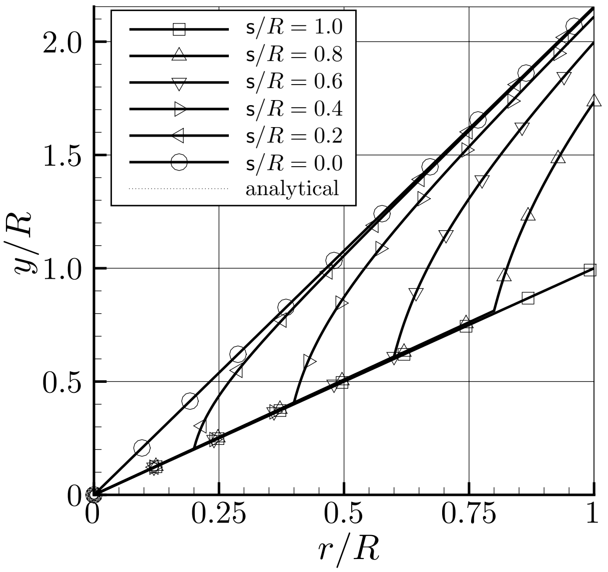

Figure 3: Normalized deformation for equally-spaced intervals of interfacial position along the gel radius.

We now examine static two-phase states for a reservoir level of $U = 1.0$ J and incremental interface positions corresponding to $\mathsf{s}/R = 1.0, 0.8, 0.6, 0.4, 0.2$, and 0.0. The dimensionless deformation y/R and diffusion potential u/Θ are shown in Figures 3 and 4. The numerical approximation for the deformation exactly reproduces the solutions (5.40) and (5.41) when the interface is fixed at $\mathsf{s} = 0$ and $\mathsf{s} = R$, respectively. For $0 < \mathsf{s} < R$, the numerical approximation for the diffusion potential is also seen to be indistinguishable from the analytically determined expression (5.42) for u. We note that when the interface is located on the interior of the specimen, its position is clearly delineated by discontinuities in both y' and u'.

Figures 5–6 depict, for the same incremental interface positions used in plotting Figures 3–4, the dimensionless radial stress $S_\parallel/(\mu_\beta - \mu_\alpha)$ and the dimensionless hoop stress $S_\perp/(\mu_\beta - \mu_\alpha)$ as functions of the dimensionless radial position r/R. These plots indicate that the collapsed phase is not stress-free. The mismatch in material moduli at the interface induces a compressive hoop stress in the swelled phase and a tensile hoop stress in the collapsed phase, as shown in Figure 6. To satisfy force balance in the bulk, this gives rise to a non-zero radial stress in the collapsed phase. Satisfaction of the bulk deformational balance then entails a non-trivial radial stress in the collapsed phase.

From Figure 5, we observe that the interfacial force balance and traction-free boundary condition are weakly enforced by the approximation. Finally, we remark that the stress components are identical in the collapsed phase, i.e., $S_\parallel = S_\perp$ for $r < \mathsf{s}$.

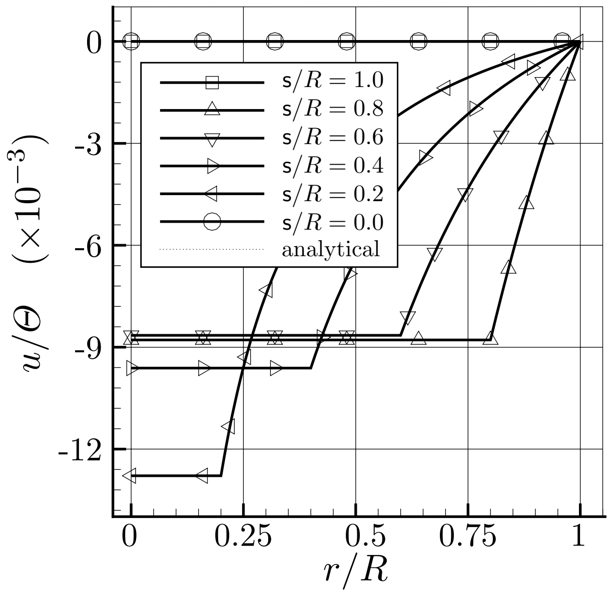

Figure 4: Normalized diffusion potential at incremental interface locations.

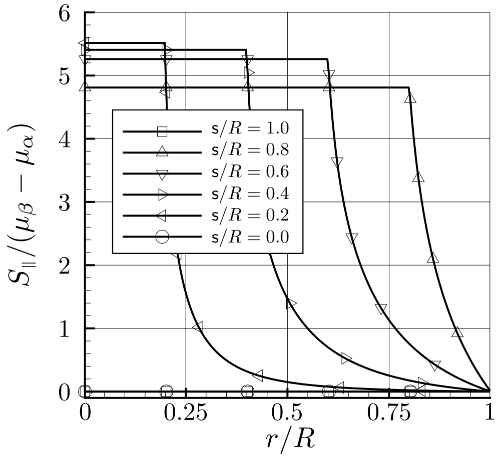

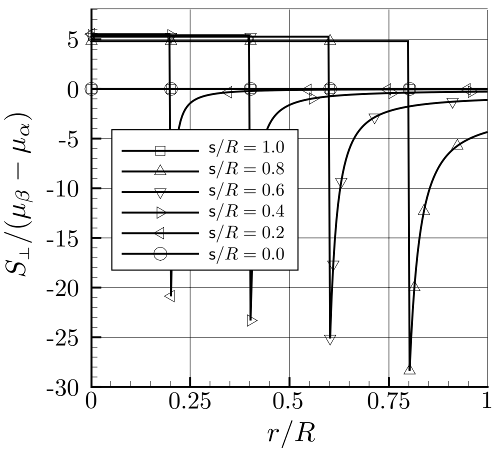

Figure 5: Normalized radial stress at incremental radial locations.

Figure 6: Normalized hoop stress at incremental interface locations.

For static two-phase states, the deformation field y/R is a nonlinear function of both the parameters J_γ and w_γ as well as the moduli μ_γ and λ_γ. It is independent of the diffusion potential U of the reservoir. To convey the complex relationships as concisely as possible, we now examine how these properties influence the swelling ratio Q as a function of s/R. Figure 7 plots $Q - Q_{\max}$ against $(\mathsf{s}/R)^3$ for various values of the parameter J_α. The curves appear to be linear, and a simple analysis yields

$$Q - Q_{\max} \approx (1 - J_\alpha)\left(\frac{\mathsf{s}}{R}\right)^3 .$$

Equivalently, since $Q_{\max} = J_\alpha$ and $Q_{\min} = 1$, we may rewrite this as

$$\frac{Q - Q_{\max}}{Q_{\min} - Q_{\max}} \approx \left(\frac{\mathsf{s}}{R}\right)^3 . \tag{5.49}$$

A plot of the deviation from this relationship is shown in Figure 8 for the same choices of J_α. Analogous studies indicate that the deviation is relatively insensitive to variations in λ_γ, μ_γ, and w_γ. The dilatation parameter J_α therefore appears to be the dominant factor in determining the swelling ratio Q.

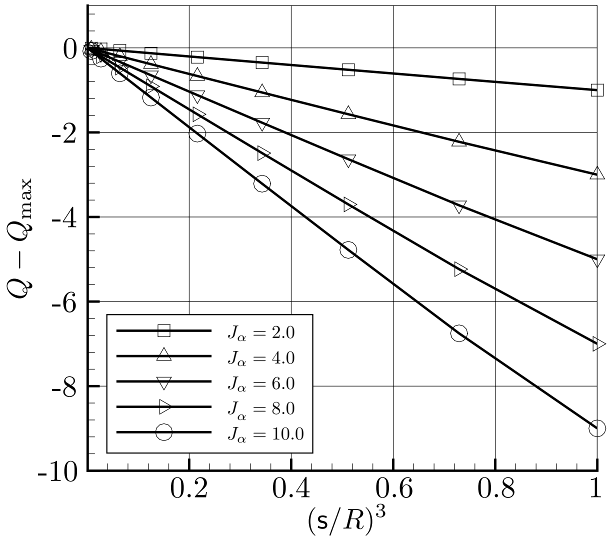

Figure 7: Influence of J_α on swelling ratio.

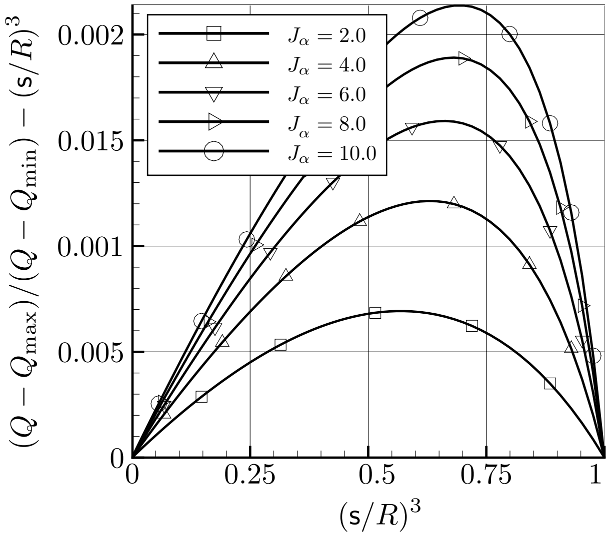

Figure 8: Deviation from scaling relationship (5.49) with various J_α.

5.5.2 Kinetics

We now present solutions to the initial-boundary-value problem (5.29)–(5.39). We begin by considering the initial and boundary conditions

$$\mathsf{s}_0 = R, \quad U = \text{constant}, \tag{5.50}$$

corresponding to a specimen that is initially collapsed, with the diffusion potential of the reservoir held constant.

As discussed in Section 5.4, the tendency for the specimen to shrink or swell depends on the difference $U - \mathsf{u}$ of the diffusion potential U of the reservoir and that u on the interface. If at some time t_* these two quantities come into balance, i.e. $\mathsf{u}(t_*) = U$, the position of the interface comes to a rest and the system reaches a state of equilibrium. Using the values of the material properties given in Table 1, we have obtained a series of solutions to the above over a range of U. Figure 9 plots the equilibrium swelling ratio Q_{eq} for this range of diffusion potential of the reservoir. We note that for U below a minimum level identified on the plot as U_{c}, the equilibrium state is identical to the initial condition specified above and the gel remains as a single collapsed phase. Above a threshold level identified as U_{th}, the equilibrium state corresponds to a gel that is fully swelled. Hereafter, we refer to such a plot as the $Q - U$ breakthrough curve.

Of the material parameters which enter our model, the $Q - U$ breakthrough curves are most sensitive to variations in J_γ, σ, and c_γ. As implied by the normalization used in Figure 9, the curves exhibit a simple scaling with the jump $[\![c_\gamma]\!]$ of the polymer concentration between the swelled and collapsed phases. If $[\![c_\gamma]\!]$ is doubled, for example, then both U_{c} and U_{th} decrease by half. The breakthrough curves for various J_α are shown in Figure 10. Clearly, increasing J_α lowers both the equilibrium diffusion potential U_{c} for the collapsed phase and threshold level U_{th} for the swelled phase. These curves were generated for the various J_α while holding the remaining material parameters fixed at the values listed in Table 1. Similar breakthrough curves for various choices of the interfacial energy density σ are shown in Figure 11. We note that a marked deviation from the curve shown in Figure 9 is only observed when the dimensionless quantity $\sigma/R[\![c_\gamma]\!]$ becomes sufficiently large.

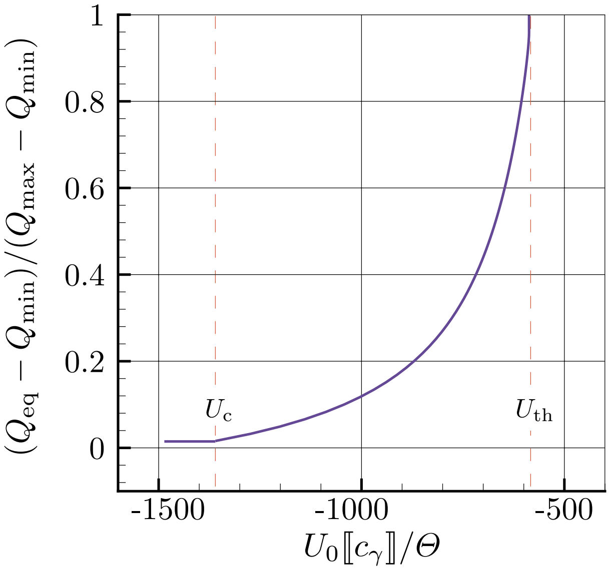

Figure 9: A "breakthrough" curve for the equilibrium swelling ratio Q_{eq} as a function of constant reservoir potential U_0. This curve is generated numerically by solving (5.52) for a sequence of different U_0. The calculations are performed for a sufficiently large interval of time such that the interface comes to an equilibrium position, yielding Q_{eq}.

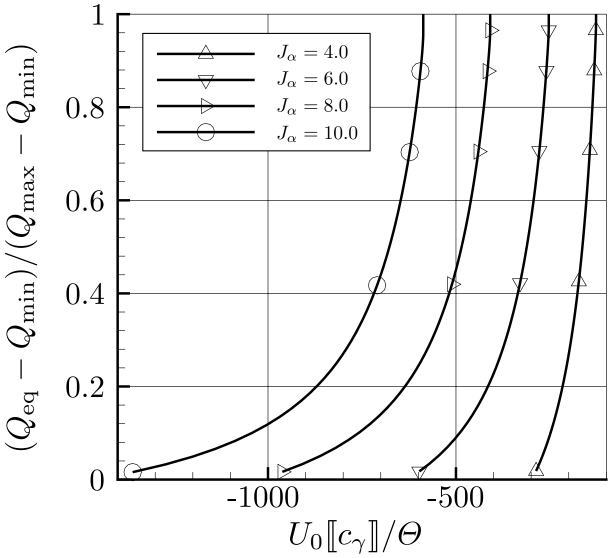

Figure 10: "Breakthrough" curves for various J_α.

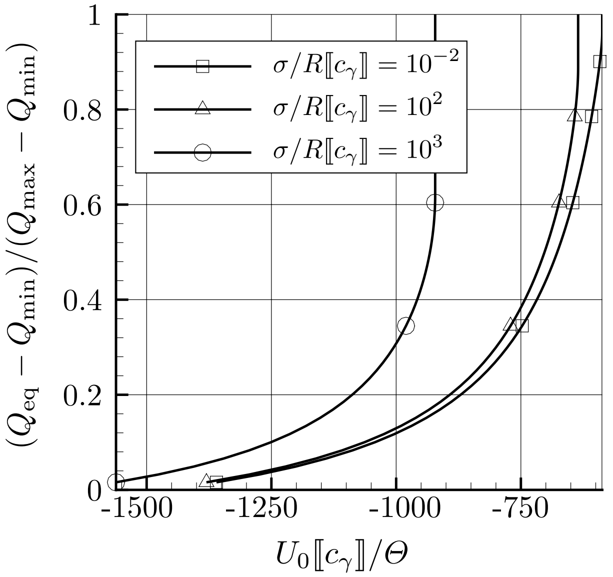

Figure 11: "Breakthrough" curves for various interfacial energy densities σ.

With the data from the above breakthrough curves, we next examine the influence of the material properties on the swelling kinetics by investigating solutions to (5.29)–(5.39) with the boundary and initial conditions

$$\mathsf{s}_0 = R, \quad U(t) = U_{\rm c} + \alpha H(t), \tag{5.51}$$

where H is the Heaviside function. These conditions correspond to a specimen that is initially in a collapsed equilibrium state and is subsequently subjected to a step change in the reservoir potential. To trigger an eventual transition to a completely swelled state, we set $\alpha = 1.05(U_{\rm th} - U_{\rm c})$. Associated with this initial-boundary-value problem we introduce a characteristic swelling time τ for the gel, defined as the time at which $\mathsf{s}(\tau) = 0$.

Figure 12 plots the dimensionless interface position as a function of dimensionless time for specimens with initial radii of 1.0 cm, 2.0 cm, 4.0 cm, and 8.0 cm. These curves were obtained using the parameter values given in Table 1 and the values of $U_{\rm c}$ and $U_{\rm th}$. We note that these curves bear a strong qualitative resemblance to the experimental results of Gehrke et al. (1992). Since $T = 100$ s, these results indicate swelling times on the order of minutes for the centimeter-scale gels. Such swelling times are also consistent with the experimental measurements of Gehrke et al. (1992).

We repeat the above calculations for the same set of initial gel radii and for $J_\alpha = 4.0, 6.0, 8.0$, and 10.0. For each J_α, the values of $U_{\rm c}$ and $U_{\rm th}$ obtained from Figure 10 are employed in (5.51). The dimensionless characteristic swelling time is plotted against the square of the gel radius in Figure 13. The results clearly indicate that $\tau \sim R^2$, with increasing J_α corresponding to faster characteristic swelling times.

As discussed in Section 5.4, the scaling $\tau \sim R^2$ is expected if the difference $U - \mathsf{u}$ is approximately constant. For comparison, Figure 14 shows the analytical prediction given by (5.47) plotted alongside the numerical results for the limiting choices of J_α. For the analytical prediction, the difference $U - \mathsf{u}$ was approximated as $U - U_{\rm th}$. The plots indicate that the analytical prediction yields swelling times that are approximately 50% longer than those obtained numerically.

The difference between the analytical and numerical predictions is attributable to the fact that $U - \mathsf{u}$ is not constant in time. A plot of this quantity, normalized by Θ, is

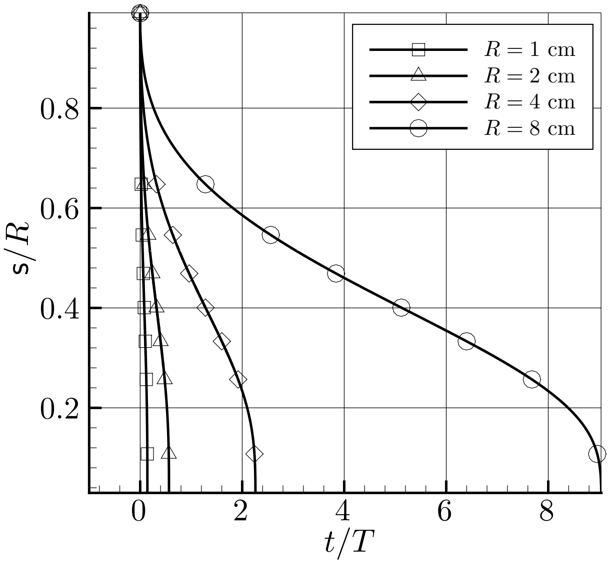

Figure 12: Normalized interface position with time for gels of increasing radii.

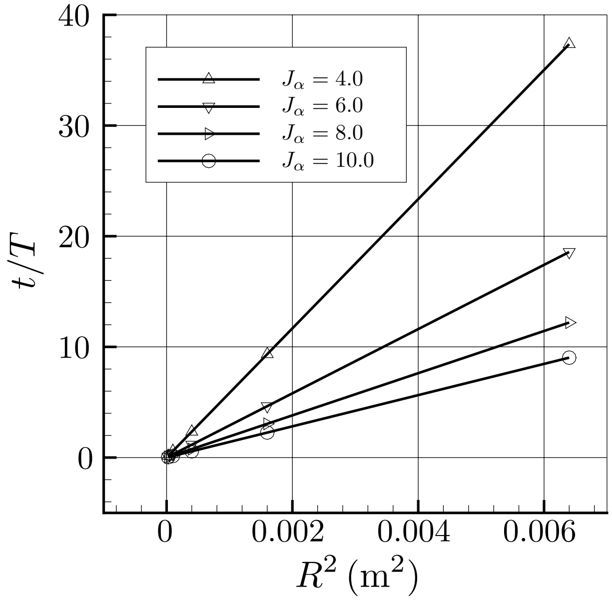

Figure 13: Characteristic swelling times as a function of initial gel radius squared for various J_α.

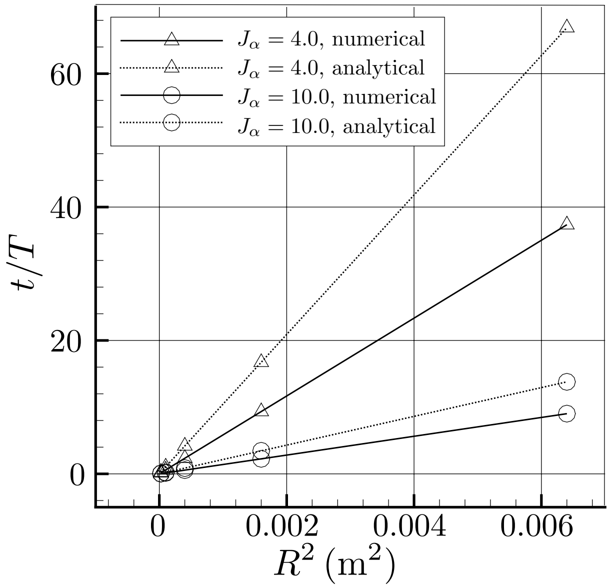

Figure 14: Comparison of numerical and analytical (5.47) characteristic swelling times.

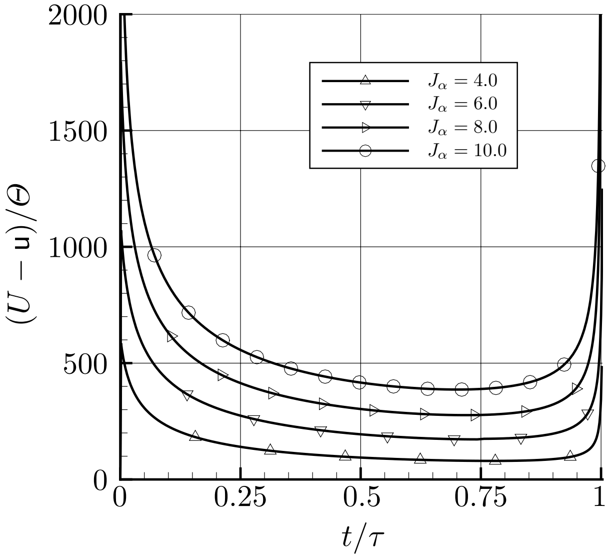

Figure 15: Diffusion potential difference as a function of time for various J_α.

shown for dimensionless time t/τ in Figure 15 for the same choices of J_α used to generate Figure 13. This plot indicates that deviations from the scaling $\tau \sim R^2$ are most likely to occur during the early and late stages of the swelling. In particular, $(U - \mathsf{u})/\Theta$ increases sharply as the characteristic swelling time τ is approached. In this regime, the interface is nearing the center of the specimen and the first term $-2\sigma/\mathsf{s}$ on the right side of (5.33) is dominant.

The characteristic swelling time τ is also sensitive to the molecular mobility m_α in the swelled phase, $\llbracket c_\gamma \rrbracket$, and σ. The influence of the mobility m_α on the characteristic swelling time follows directly from (5.44). Doubling the mobility in the swelled phase simply doubles the velocity of the interface, and therefore decreases the swelling time by a factor of two. Similarly, the interface velocity is inversely proportional to the jump $\llbracket c_\gamma \rrbracket$ in polymer chain concentration. As discussed above, the levels U_{c} and U_{th} are also inversely proportional to $\llbracket c_\gamma \rrbracket$. It follows that the characteristic swelling times obtained using (5.51) are proportional to $1/\llbracket c_\gamma \rrbracket^2$.

The interfacial energy density σ does not influence the scaling $\tau \sim R^2$ until the ratio σ/R becomes sufficiently large. The effect is akin to surface tension dominating the local force balance of fluid interfaces at small length scales. In Figure 16, the dimensionless characteristic swelling time t/τ is displayed for various choices of $\sigma/R\llbracket c_\gamma \rrbracket$. We note the slight deviation from $\tau \sim R^2$ for sufficiently large σ. In Figure 17, plots of the dimensionless difference $(U - \mathsf{u})/\Theta$ of the diffusion potential of the reservoir and the diffusion potential on the interface are shown for the same choices of $\sigma/R\llbracket c_\gamma \rrbracket$ used in generating Figure 16. As σ is increased, so too does the variation in $U - \mathsf{u}$. Although we observe some deviation from $\tau \sim R^2$ for these cases, the associated magnitude of σ appears artificially large.

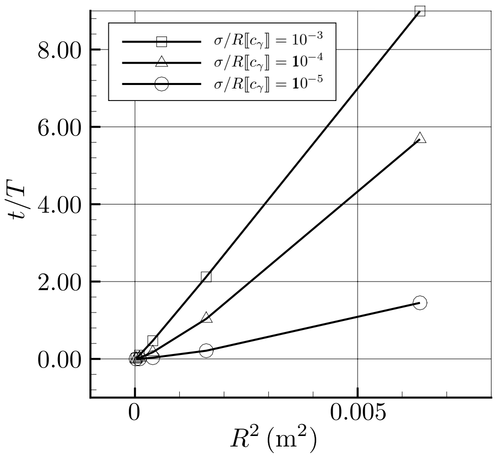

Figure 16: Characteristic swelling times as a function of initial gel radius squared for various σ.

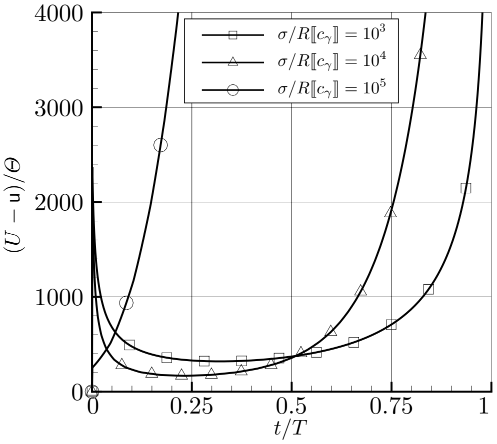

Figure 17: Diffusion potential difference as a function of time for various σ.

5.5.3 Response to Cyclic Loading

We now consider solutions to (5.29)–(5.39) with the initial and boundary conditions

$$\mathsf{s}_0 = R, \quad U(t + T_*) = U(t), \tag{5.52}$$

corresponding to an initially collapsed specimen that is subjected to a cyclic variation, with period T_*, of the diffusion potential U of the reservoir. In particular, we discuss the response to a sawtooth cycle with amplitude Θ_* and minimum U_0 (Figure 18).

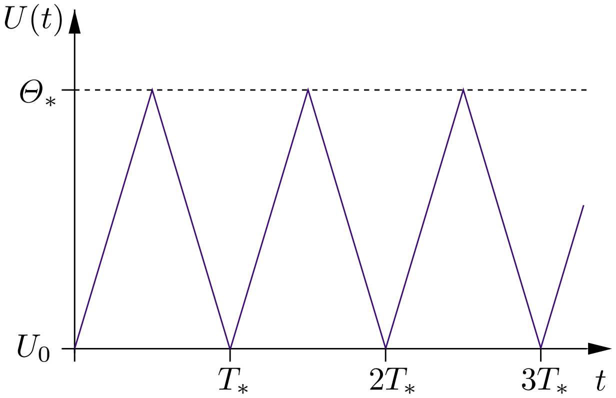

Figure 18: Excitation of diffusion potential on gel surface with period T and height Θ.

As U oscillates between U_c and U_th, our model predicts a hysteretic response in the swelling ratio Q. To illustrate this, we consider the case where the minimum diffusion potential of the reservoir is given by $U_0 = U_\mathrm{c} + 0.40(U_\mathrm{th} - U_\mathrm{c})$, $\Theta = 0.75(U_\mathrm{th} - U_\mathrm{c})$, and $T_* = \tau/10$. The swelling ratio Q is plotted against U in Figure 19. Subsequent to an initial transient, the material response enters a limit cycle. Figure 20 compares the diffusion potential on the boundary to that of the interface. The situation $U > \mathsf{u}$ corresponds to increasing Q and similarly $U < \mathsf{u}$ to decreasing Q. We note that although the diffusion potential of the reservoir exceeds the threshold U_th, the period T_* of the cycle is not large enough to trigger total swelling. From Figure 20, it appears that the minimum of the diffusion potential u on the interface is shifted away from that of the reservoir. In other words, there is a short interval of time during which U is increasing with time while u is still decreasing. During this interval the interface is still moving toward the boundary of the specimen, because $U < \mathsf{u}$.

6 Summary and concluding remarks

With the emergence of technologies that rely on the novel swelling behavior of hydrogels comes a convincing need for physically accurate theories and numerical simulations capable of capturing analyzing and predicting this behavior. To design micro-actuation and sensing devices based on hydrogels, for example, predictions of swelling times and available force densities will be critical. By the same token, purely phenomenological or empirical models do not provide sufficient physical links to the various processes associated with the swelling of hydrogels. Without such links, the performance characteristics of the gels cannot be “optimized” during fabrication.

Motivated by the above as well as recent experimental observations, we present a new theory for describing the chemo-mechanical swelling behavior of hydrogels. This

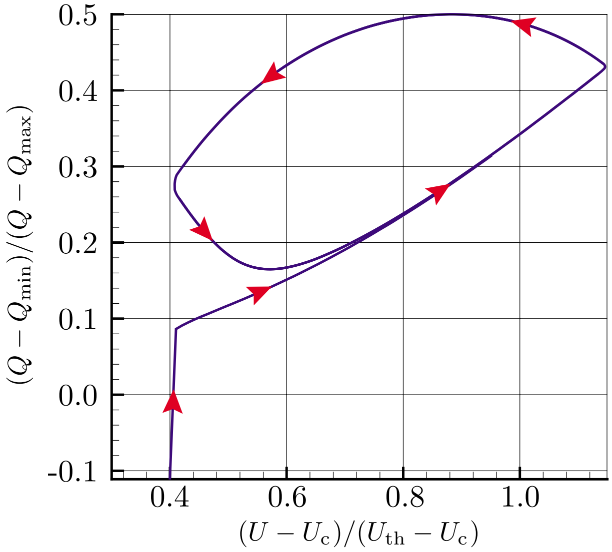

Figure 19: Swelling ratio vs. reservoir potential. Arrows indicate the direction of increasing time.

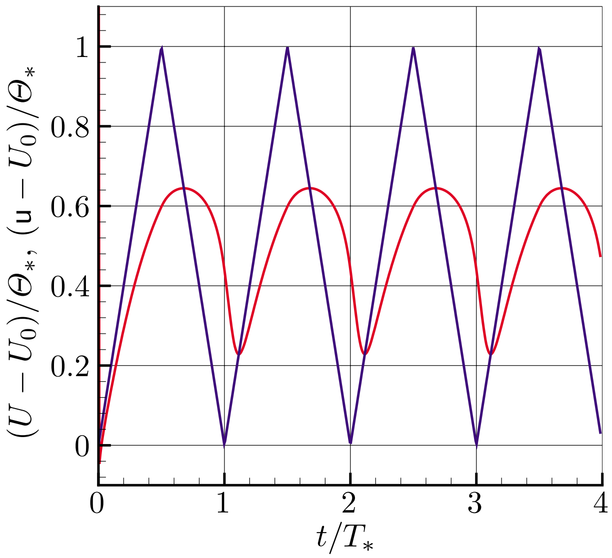

Figure 20: Temporal variations of the diffusion potential of the reservoir and the diffusion potential on the interface.

theory models the interface separating the swelled and collapsed phases of the gel by a sharp surface of discontinuity. The polymer chains are treated as a solute with an associated diffusion potential, and their concentration is assumed to be discontinuous across the interface. The governing equations for the bulk phases and the interface are then obtained by considering deformational force balance, configurational force balance, and solute balance. A bulk dissipation imbalance, which represents the first and second laws under isothermal conditions, is also imposed as a means to provide restrictions on constitutive equations.

As an approximation, the theory is specialized to the situation in which the motion of the interface is slow compared to the diffusion in the bulk phases, as is suggested by the experimental observations of Gehrke et al. (1992). This results a system of governing equations where the coupling between the deformation and solute concentration is solely through the normal configurational force balance which holds across the interface. This system of evolution equations is then recast into an equivalent, hybrid variational form, with the interfacial solute balance viewed within the framework of the level-set method. We describe suitable approximations for the deformation and diffusion potential in the context of the eXtended-Finite-Element/Level-Set Method (XFE/LSM). In particular, local enrichment functions are employed to capture the discontinuities in the gradients of the primary fields at the interface.

Finally, to ilustrate some features of the theory and its numerical approximation, the swelling of a spherical specimen is studied. We consider a specimen whose boundary is traction-free and is in contact with a reservoir of uniform chemical potential. To capture the dramatic volume changes associated with swelling and collapse, we rely on a strain-energy function which depends on the energetically preferred dilatation for each phase. A series of parametric studies indicate good qualitative agreement with experimental observations. Most notably, we predict characteristic swelling times that are proportional to the square of the initial gel radius for a wide range of material properties. Previous models that provided this result were based upon the assumption of collective diffusion, which assumes that swelling occurs spontaneously throughout the material. In a further departure from models based on the notion of collective diffusion, our model also predicts a hysteretic response in the swelling ratio to cyclic variations of the diffusion potential in the reservoir.

From the perspecitive of materials design, several key conclusions can be extracted from our results. In particular, the results suggest that the response time for swelling can be decreased in at least three ways:

(*i*) by designing the underlying polymer network such that the preferred dilatation J_α in the swelled phase is as large as possible;

(*ii*) by increasing the mobility of the polymer chains in the swelled phase; and

(*iii*) by adjusting the solvent such that the jump $[\![c_\gamma]\!]$ in polymer concentration between swelled and collapsed phases is maximized.

Obviously, a number of the above properties may not be independent, and only a detailed comparison with careful experiments will reveal the fidelity of our predictions.

We also remark that many stimulus-responsive gels swell in response to changes in pH or temperature and that our framework could easily be extended to account for these effects.

As a caveat to the foregoing remarks, we emphasize that the assumption that the time scale for swelling is much slower than that for bulk diffusion and the particular constitive equations that we use may limit the applicability of our model. Further studies are necessary to determine the extent and nature of any such limitations.

Furthermore, our treatment of the boundary conditions for the gel surface neglects effects such as surface tension and the exchange of material, effects which may be central to the understanding of wrinkling and other surface patterns. Extension of the theory to account for such effects and numerical studies of two-dimensional problems is therefore necessary.

References

Bai, G. and A. Suzuki (2000). Shrinking patterns and phase coexistence of polymer gels. *Materials and Design 21*, 547–550.

Beebe, D. J., J. S. Moore, J. M. Bauer, Q. Yu, R. H. Liu, C. Devadoss, and B. Jo (2000). Functional hydrogel structures for autonomous flow control inside microfluidic channels. *Nature 404*, 588–590.

Budtova, T. (1998). Absoprtion/release of polyvalent metal ions by a polyelectrolyte gel. *Journal of Controlled Release 54*(3), 305–312.

Budtova, T. and P. Navard (1998). Swelling kinetics of polyelectrolyte gel in water and salt solutions. Coexistence of swollen and collapsed phases. *Macromolecules 31*(25), 8845–8850.

Chopp, D. L. (2001). Some improvements of the fast marching method. *SIAM Journal on Scientific Computing 23*(1), 230–244.

Dolbow, J. (1999). *An extended finite element method with discontinuous enrichment for applied mechanics*. Ph. D. thesis, Northwestern University.

Dolbow, J., N. Moës, and T. Belytschko (2000). Discontinuous enrichment in finite elements with a partition of unity method. *Finite Elements in Analysis and Design 36*, 235–260.

Dolbow, J., N. Moës, and T. Belytschko (2001). An extended finite element method for modeling crack growth with frictional contact. *Computer Methods in Applied Mechanics and Engineering 190*, 6825–6846.

Dušek, K. (Ed.) (1993). *Responsive Gels: Volume Transitions I, Advances in Polymer Science*, Volume 109, Berlin. Springer.

Eichenbaum, G. M., P. F. Kiser, D. Shah, S. A. Simon, and D. Needham (1999). Investigation of the swelling response and drug loading of ionic microgels: The dependence on functional group composition. *Macromolecules 32*, 8996–9006.

Fried, E. and M. E. Gurtin (1999). Coherent solid-state phase transitions with atomic diffusion: A thermomechanical treatment. *Journal of Statistical Physics 95*(5–6), 1361–1427.

Gehrke, S. H., G. Agrawal, and M. C. Yang (1992). Moving ion exchange fronts in polyelectrolyte gels. *ACS Symposium Series 480*, 211–237.

Gibbs, J. W. (1878). On the equilibrium of heterogeneous substances. *Transactions of the Connecticut Academy of Arts and Sciences 3*, 108–248.

Gurtin, M. E. (1995). The nature of configurational forces. *Archive for Rational Mechanics and Analysis 131*(1), 67–100.

Gurtin, M. E. (2000). *Configurational Forces as Basic Concepts in Continuum Physics.* New York: Springer.

Gurtin, M. E. and A. Struthers (1990). Evolving phase boundaries in the presence of bulk deformation. *Archive for Rational Mechanics and Analysis 112*, 97–160.

Gurtin, M. E. and P. W. Voorhees (1993). The continuum mechanics of coherent two-phase elastic solids with mass transport. *Proceedings of the Royal Society of London Series A 440*(1909), 323–343.

Ji, H. (2001). A note on enrichment functions for gradient discontinuities. Technical Report 1, Department of Civil Engineering, Duke University.

Ji, H., D. Chopp, and J. E. Dolbow (2002). A hybrid extended finite element/ level set method for modeling phase transformations. *International Journal for Numerical Methods in Engineering 54*, 1209–1233.

Krongauz, Y. and T. Belytschko (1998). EFG approximation with discontinuous derivatives. *International Journal for Numerical Methods in Engineering 41*(7), 1215–1233.

Lynch, D. and K. O'Neill (1981). Continuously deforming finite elements for the solution of parabolic problems, with and without phase change. *International Journal for Numerical Methods in Engineering 17*, 81–96.

Matsuo, E. and T. Tanaka (1989). Kinetics of discontinuous volume phase-transition of gels. *Journal of Chemical Physics 89*(3), 1695–1703.

Melenk, J. M. and I. Babuška (1996). The partition of unity finite element method: Basic theory and applications. *Computer Methods in Applied Mechanics and Engineering 139*, 289–314.

Merle, R. and J. Dolbow (2002). Solving thermal and phase change problems with the extended finite element method. *Computational Mechanics 28*, 339–350.

Moës, N., J. Dolbow, and T. Belytschko (1999). A finite element method for crack growth without remeshing. *International Journal for Numerical Methods in Engineering 46*, 131–150.

Mullins, W. and R. Sekerka (1963). Morphological stability of a particle growing by diffusion and heat flow. *Journal of Applied Physics 34*, 323–329.

Olsen, M., J. M. Bauer, and D. Beebe (2000). Particle imaging techniques for measuring the deformation rate of hydrogel microstructures. *Applied Physics Letters 76*(22), 3310–3312.

Onuki, A. (1993). Theory of phase transition in polymer gels. In K. Dušek (Ed.), *Responsive Gels: Volume Transitions I, Advances in Polymer Science*, Volume 109, Berlin, pp. 63–121. Springer.

Osher, S. and J. Sethian (1988). Fronts propagating with curvature dependent speed: Algorithms based on Hamilton-Jacobi formulation. *Journal of Computational Physics 79*, 12–49.

Sethian, J. (1996). *Level Set Methods and Fast Marching Methods*. New York, NY: Cambridge University Press.

Sukumar, N., D. Chopp, N. Moës, and T. Belytschko (2001). Modeling holes and inclusions by level sets in the extended finite element method. *Computer Methods in Applied Mechanics and Engineering 190*, 6183–6200.

Tanaka, T. (1978). Collapse of gels and critical endpoint. *Physical Review Letters 40*(12), 820–823.

Tanaka, T., L. Hocker, and G. B. Benedek (1973). Spectrum of light scattered from a viscoelastic gel. *Journal of Chemical Physics 59*, 5151–5159.

Tanaka, T., E. Sato, Y. Hirokawa, S. Hirotsu, and J. Peetermans (1985). Critical kinetics of volume phase-transitions of gels. *Physical Review Letters 55*(22), 2455–2458.

Tanaka, T., S. T. Sun, Y. Hirokawa, S. Katayama, J. Kucera, Y. Hirose, and T. Amiya (1987). Mechanical instability of gels at the phase transition. *Nature 325*(6107), 796–798.

Tomari, T. and M. Doi (1994). Swelling dnamics of a gel undergoing volume transitions. *Journal of the Physical Society of Japan 63*(6), 2093–2101.

Tomari, T. and M. Doi (1995). Hysteresis and incubation in the dynamics of volume transition of spherical gels. *Macromolecules 28*, 8334–8343.

Udaykumar, H., R. Mittal, and W. Shyy (1999). Computation of solid-liquid phase fronts in the sharp interface limit on fixed grids. *Journal of Computational Physics 153*, 535–574.

List of Recent TAM Reports

No.	*Authors*	*Title*	*Date*
933	Sakakibara, J., Hishida, K., and W. R. C. Phillips	On the vortical structure in a plane impinging jet—*Journal of Fluid Mechanics* **434**, 273–300 (2001)	Apr. 2000
934	Phillips, W. R. C.	Eulerian space–time correlations in turbulent shear flows—*Physics of Fluids* **12**, 2056–2064 (2000)	Apr. 2000
935	Hsui, A. T., and D. N. Riahi	Onset of thermal–chemical convection with crystallization within a binary fluid and its geological implications—*Geochemistry, Geophysics, Geosystems* **2**, 2000GC000075 (2001)	Apr. 2000
936	Cermelli, P., E. Fried, and S. Sellers	Configurational stress, yield, and flow in rate-independent plasticity—*Proceedings of the Royal Society of London A* **457**, 1447–1467 (2001)	Apr. 2000
937	Adrian, R. J., C. Meneveau, R. D. Moser, and J. J. Riley	Final report on 'Turbulence Measurements for Large-Eddy Simulation' workshop	Apr. 2000
938	Bagchi, P., and S. Balachandar	Linearly varying ambient flow past a sphere at finite Reynolds number—Part 1: Wake structure and forces in steady straining flow	Apr. 2000
939	Gioia, G., A. DeSimone, M. Ortiz, and A. M. Cuitiño	Folding energetics in thin-film diaphragms—*Proceedings of the Royal Society of London A* **458**, 1223–1229 (2002)	Apr. 2000
940	Chaïeb, S., and G. H. McKinley	Mixing immiscible fluids: Drainage induced cusp formation	May 2000
941	Thoroddsen, S. T., and A. Q. Shen	Granular jets—*Physics of Fluids* **13**, 4–6 (2001)	May 2000
942	Riahi, D. N.	Non-axisymmetric chimney convection in a mushy layer under a high-gravity environment—In *Centrifugal Materials Processing* (L. L. Regel and W. R. Wilcox, eds.), 295–302 (2001)	May 2000
943	Christensen, K. T., S. M. Soloff, and R. J. Adrian	PIV Sleuth: Integrated particle image velocimetry interrogation/validation software	May 2000
944	Wang, J., N. R. Sottos, and R. L. Weaver	Laser induced thin film spallation—*Experimental Mechanics* (submitted)	May 2000
945	Riahi, D. N.	Magnetohydrodynamic effects in high gravity convection during alloy solidification—In *Centrifugal Materials Processing* (L. L. Regel and W. R. Wilcox, eds.), 317–324 (2001)	June 2000
946	Gioia, G., Y. Wang, and A. M. Cuitiño	The energetics of heterogeneous deformation in open-cell solid foams—*Proceedings of the Royal Society of London A* **457**, 1079–1096 (2001)	June 2000
947	Kessler, M. R., and S. R. White	Self-activated healing of delamination damage in woven composites—*Composites A: Applied Science and Manufacturing* **32**, 683–699 (2001)	June 2000
948	Phillips, W. R. C.	On the pseudomomentum and generalized Stokes drift in a spectrum of rotational waves—*Journal of Fluid Mechanics* **430**, 209–229 (2001)	July 2000
949	Hsui, A. T., and D. N. Riahi	Does the Earth's nonuniform gravitational field affect its mantle convection?—*Physics of the Earth and Planetary Interiors* (submitted)	July 2000
950	Phillips, J. W.	Abstract Book, 20th International Congress of Theoretical and Applied Mechanics (27 August – 2 September, 2000, Chicago)	July 2000
951	Vainchtein, D. L., and H. Aref	Morphological transition in compressible foam—*Physics of Fluids* **13**, 2152–2160 (2001)	July 2000
952	Chaïeb, S., E. Sato-Matsuo, and T. Tanaka	Shrinking-induced instabilities in gels	July 2000
953	Riahi, D. N., and A. T. Hsui	A theoretical investigation of high Rayleigh number convection in a nonuniform gravitational field—*International Journal of Pure and Applied Mathematics*, in press (2003)	Aug. 2000

List of Recent TAM Reports (cont'd)

No.	*Authors*	*Title*	*Date*
954	Riahi, D. N.	Effects of centrifugal and Coriolis forces on a hydromagnetic chimney convection in a mushy layer—*Journal of Crystal Growth* **226**, 393–405 (2001)	Aug. 2000
955	Fried, E.	An elementary molecular-statistical basis for the Mooney and Rivlin–Saunders theories of rubber-elasticity—*Journal of the Mechanics and Physics of Solids* **50**, 571–582 (2002)	Sept. 2000
956	Phillips, W. R. C.	On an instability to Langmuir circulations and the role of Prandtl and Richardson numbers—*Journal of Fluid Mechanics* **442**, 335–358 (2001)	Sept. 2000
957	Chaïeb, S., and J. Sutin	Growth of myelin figures made of water soluble surfactant—Proceedings of the 1st Annual International IEEE–EMBS Conference on Microtechnologies in Medicine and Biology (October 2000, Lyon, France), 345–348	Oct. 2000
958	Christensen, K. T., and R. J. Adrian	Statistical evidence of hairpin vortex packets in wall turbulence—*Journal of Fluid Mechanics* **431**, 433–443 (2001)	Oct. 2000
959	Kuznetsov, I. R., and D. S. Stewart	Modeling the thermal expansion boundary layer during the combustion of energetic materials—*Combustion and Flame*, in press (2001)	Oct. 2000
960	Zhang, S., K. J. Hsia, and A. J. Pearlstein	Potential flow model of cavitation-induced interfacial fracture in a confined ductile layer—*Journal of the Mechanics and Physics of Solids*, **50**, 549–569 (2002)	Nov. 2000
961	Sharp, K. V., R. J. Adrian, J. G. Santiago, and J. I. Molho	Liquid flows in microchannels—Chapter 6 of *CRC Handbook of MEMS* (M. Gad-el-Hak, ed.) (2001)	Nov. 2000
962	Harris, J. G.	Rayleigh wave propagation in curved waveguides—*Wave Motion* **36**, 425–441 (2002)	Jan. 2001
963	Dong, F., A. T. Hsui, and D. N. Riahi	A stability analysis and some numerical computations for thermal convection with a variable buoyancy factor—*Journal of Theoretical and Applied Mechanics* **2**, 19–46 (2002)	Jan. 2001
964	Phillips, W. R. C.	Langmuir circulations beneath growing or decaying surface waves—*Journal of Fluid Mechanics* (submitted)	Jan. 2001
965	Bdzil, J. B., D. S. Stewart, and T. L. Jackson	Program burn algorithms based on detonation shock dynamics—*Journal of Computational Physics* (submitted)	Jan. 2001
966	Bagchi, P., and S. Balachandar	Linearly varying ambient flow past a sphere at finite Reynolds number: Part 2—Equation of motion—*Journal of Fluid Mechanics* (submitted)	Feb. 2001
967	Cermelli, P., and E. Fried	The evolution equation for a disclination in a nematic fluid—*Proceedings of the Royal Society A* **458**, 1–20 (2002)	Apr. 2001
968	Riahi, D. N.	Effects of rotation on convection in a porous layer during alloy solidification—Chapter 12 in *Transport Phenomena in Porous Media* (D. B. Ingham and I. Pop, eds.), 316–340 (2002)	Apr. 2001
969	Damljanovic, V., and R. L. Weaver	Elastic waves in cylindrical waveguides of arbitrary cross section—*Journal of Sound and Vibration* (submitted)	May 2001
970	Gioia, G., and A. M. Cuitiño	Two-phase densification of cohesive granular aggregates—*Physical Review Letters* **88**, 204302 (2002) (in extended form and with added co-authors S. Zheng and T. Uribe)	May 2001
971	Subramanian, S. J., and P. Sofronis	Calculation of a constitutive potential for isostatic powder compaction—*International Journal of Mechanical Sciences* (submitted)	June 2001
972	Sofronis, P., and I. M. Robertson	Atomistic scale experimental observations and micromechanical/continuum models for the effect of hydrogen on the mechanical behavior of metals—*Philosophical Magazine* (submitted)	June 2001
973	Pushkin, D. O., and H. Aref	Self-similarity theory of stationary coagulation—*Physics of Fluids* **14**, 694–703 (2002)	July 2001

List of Recent TAM Reports (cont'd)

No.	*Authors*	*Title*	*Date*
974	Lian, L., and N. R. Sottos	Stress effects in ferroelectric thin films—*Journal of the Mechanics and Physics of Solids* (submitted)	Aug. 2001
975	Fried, E., and R. E. Todres	Prediction of disclinations in nematic elastomers—*Proceedings of the National Academy of Sciences* **98**, 14773–14777 (2001)	Aug. 2001
976	Fried, E., and V. A. Korchagin	Striping of nematic elastomers—*International Journal of Solids and Structures* **39**, 3451–3467 (2002)	Aug. 2001
977	Riahi, D. N.	On nonlinear convection in mushy layers: Part I. Oscillatory modes of convection—*Journal of Fluid Mechanics* **467**, 331–359 (2002)	Sept. 2001
978	Sofronis, P., I. M. Robertson, Y. Liang, D. F. Teter, and N. Aravas	Recent advances in the study of hydrogen embrittlement at the University of Illinois—Invited paper, Hydrogen–Corrosion Deformation Interactions (Sept. 16–21, 2001, Jackson Lake Lodge, Wyo.)	Sept. 2001
979	Fried, E., M. E. Gurtin, and K. Hutter	A void-based description of compaction and segregation in flowing granular materials—*Proceedings of the Royal Society of London A* (submitted)	Sept. 2001
980	Adrian, R. J., S. Balachandar, and Z.-C. Liu	Spanwise growth of vortex structure in wall turbulence—*Korean Society of Mechanical Engineers International Journal* **15**, 1741–1749 (2001)	Sept. 2001
981	Adrian, R. J.	Information and the study of turbulence and complex flow—*Japanese Society of Mechanical Engineers Journal B*, in press (2002)	Oct. 2001
982	Adrian, R. J., and Z.-C. Liu	Observation of vortex packets in direct numerical simulation of fully turbulent channel flow—*Journal of Visualization*, in press (2002)	Oct. 2001
983	Fried, E., and R. E. Todres	Disclinated states in nematic elastomers—*Journal of the Mechanics and Physics of Solids* **50**, 2691–2716 (2002)	Oct. 2001
984	Stewart, D. S.	Towards the miniaturization of explosive technology—Proceedings of the 23rd International Conference on Shock Waves (2001)	Oct. 2001
985	Kasimov, A. R., and Stewart, D. S.	Spinning instability of gaseous detonations—*Journal of Fluid Mechanics* (submitted)	Oct. 2001
986	Brown, E. N., N. R. Sottos, and S. R. White	Fracture testing of a self-healing polymer composite—*Experimental Mechanics* (submitted)	Nov. 2001
987	Phillips, W. R. C.	Langmuir circulations—*Surface Waves* (J. C. R. Hunt and S. Sajjadi, eds.), in press (2002)	Nov. 2001
988	Gioia, G., and F. A. Bombardelli	Scaling and similarity in rough channel flows—*Physical Review Letters* **88**, 014501 (2002)	Nov. 2001
989	Riahi, D. N.	On stationary and oscillatory modes of flow instabilities in a rotating porous layer during alloy solidification—*Journal of Porous Media*, in press (2002)	Nov. 2001
990	Okhuysen, B. S., and D. N. Riahi	Effect of Coriolis force on instabilities of liquid and mushy regions during alloy solidification—*Physics of Fluids* (submitted)	Dec. 2001
991	Christensen, K. T., and R. J. Adrian	Measurement of instantaneous Eulerian acceleration fields by particle-image accelerometry: Method and accuracy—*Experimental Fluids* (submitted)	Dec. 2001
992	Liu, M., and K. J. Hsia	Interfacial cracks between piezoelectric and elastic materials under in-plane electric loading—*Journal of the Mechanics and Physics of Solids* **51**, 921–944 (2003)	Dec. 2001
993	Panat, R. P., S. Zhang, and K. J. Hsia	Bond coat surface rumpling in thermal barrier coatings—*Acta Materialia* **51**, 239–249 (2003)	Jan. 2002
994	Aref, H.	A transformation of the point vortex equations—*Physics of Fluids* **14**, 2395–2401 (2002)	Jan. 2002
995	Saif, M. T. A, S. Zhang, A. Haque, and K. J. Hsia	Effect of native Al_2O_3 on the elastic response of nanoscale aluminum films—*Acta Materialia* **50**, 2779–2786 (2002)	Jan. 2002
996	Fried, E., and M. E. Gurtin	A nonequilibrium theory of epitaxial growth that accounts for surface stress and surface diffusion—*Journal of the Mechanics and Physics of Solids*, in press (2002)	Jan. 2002

List of Recent TAM Reports (cont'd)

No.	*Authors*	*Title*	*Date*
997	Aref, H.	The development of chaotic advection—*Physics of Fluids* **14**, 1315–1325 (2002); see also *Virtual Journal of Nanoscale Science and Technology*, 11 March 2002	Jan. 2002
998	Christensen, K. T., and R. J. Adrian	The velocity and acceleration signatures of small-scale vortices in turbulent channel flow—*Journal of Turbulence*, in press (2002)	Jan. 2002
999	Riahi, D. N.	Flow instabilities in a horizontal dendrite layer rotating about an inclined axis—*Proceedings of the Royal Society of London A* (submitted)	Feb. 2002
1000	Kessler, M. R., and S. R. White	Cure kinetics of ring-opening metathesis polymerization of dicyclopentadiene—*Journal of Polymer Science A* **40**, 2373–2383 (2002)	Feb. 2002
1001	Dolbow, J. E., E. Fried, and A. Q. Shen	Point defects in nematic gels: The case for hedgehogs—*Proceedings of the National Academy of Sciences* (submitted)	Feb. 2002
1002	Riahi, D. N.	Nonlinear steady convection in rotating mushy layers—*Journal of Fluid Mechanics*, in press (2003)	Mar. 2002
1003	Carlson, D. E., E. Fried, and S. Sellers	The totality of soft-states in a neo-classical nematic elastomer—*Proceedings of the Royal Society A* (submitted)	Mar. 2002
1004	Fried, E., and R. E. Todres	Normal-stress differences and the detection of disclinations in nematic elastomers—*Journal of Polymer Science B: Polymer Physics* **40**, 2098–2106 (2002)	June 2002
1005	Fried, E., and B. C. Roy	Gravity-induced segregation of cohesionless granular mixtures—*Lecture Notes in Mechanics*, in press (2002)	July 2002
1006	Tomkins, C. D., and R. J. Adrian	Spanwise structure and scale growth in turbulent boundary layers—*Journal of Fluid Mechanics* (submitted)	Aug. 2002
1007	Riahi, D. N.	On nonlinear convection in mushy layers: Part 2. Mixed oscillatory and stationary modes of convection—*Journal of Fluid Mechanics* (submitted)	Sept. 2002
1008	Aref, H., P. K. Newton, M. A. Stremler, T. Tokieda, and D. L. Vainchtein	Vortex crystals—*Advances in Applied Mathematics* **39**, in press (2002)	Oct. 2002
1009	Bagchi, P., and S. Balachandar	Effect of turbulence on the drag and lift of a particle—*Physics of Fluids* (submitted)	Oct. 2002
1010	Zhang, S., R. Panat, and K. J. Hsia	Influence of surface morphology on the adhesive strength of aluminum/epoxy interfaces—*Journal of Adhesion Science and Technology* (submitted)	Oct. 2002
1011	Carlson, D. E., E. Fried, and D. A. Tortorelli	On internal constraints in continuum mechanics—*Journal of Elasticity* (submitted)	Oct. 2002
1012	Boyland, P. L., M. A. Stremler, and H. Aref	Topological fluid mechanics of point vortex motions—*Physica D* **175**, 69–95 (2002)	Oct. 2002
1013	Bhattacharjee, P., and D. N. Riahi	Computational studies of the effect of rotation on convection during protein crystallization—*Journal of Crystal Growth* (submitted)	Feb. 2003
1014	Brown, E. N., M. R. Kessler, N. R. Sottos, and S. R. White	*In situ* poly(urea-formaldehyde) microencapsulation of dicyclopentadiene—*Journal of Microencapsulation* (submitted)	Feb. 2003
1015	Brown, E. N., S. R. White, and N. R. Sottos	Microcapsule induced toughening in a self-healing polymer composite—*Journal of Materials Science* (submitted)	Feb. 2003
1016	Kuznetsov, I. R., and D. S. Stewart	Burning rate of energetic materials with thermal expansion—*Combustion and Flame* (submitted)	Mar. 2003
1017	Dolbow, J., E. Fried, and H. Ji	Chemically induced swelling of hydrogels—*Journal of the Mechanics and Physics of Solids* (submitted)	Mar. 2003